Cell

Article

Orphan quality control shapes network dynamics and gene expression

Graphical abstract

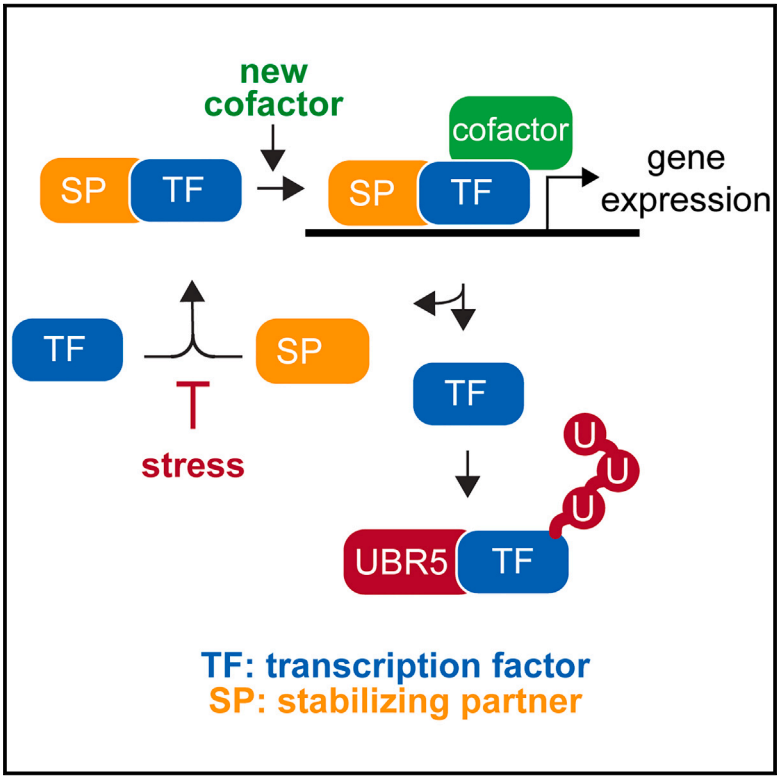

Authors

Kevin G. Mark, SriDurgaDevi Kolla, Jacob D. Aguirre, ..., Stephanie K. See, Nicolas H. Thomä, Michael Rapé

Correspondence

nicolas.thoma@fmi.ch (N.H.T.), mrape@berkeley.edu (M.R.)

In brief

Cells use orphan quality control to constantly degrade unpaired transcription factor subunits and, thereby, establish dynamic protein interaction networks that drive accurate gene expression and cell fate determination.

Highlights

- The E3 ligase UBR5 targets many transcription factors that cooperate with c-Myc
- UBR5 selectively recognizes unpaired transcription factor subunits
- Substrate sandwiching by tetrameric UBR5 establishes specificity for unpaired subunits
- Orphan degradation establishes dynamic interaction networks driving gene expression

Mark et al., 2023, Cell *186*, 3460–3475
August 3, 2023
https://doi.org/10.1016/j.cell.2023.06.015

CellPress

CellPress
OPEN ACCESS

Cell

Article

Orphan quality control shapes network dynamics and gene expression

Kevin G. Mark,[1,6] SriDurgaDevi Kolla,[1,6] Jacob D. Aguirre,[2,6] Danielle M. Garshott,[1,7] Stefan Schmitt,[2,7] Diane L. Haakonsen,[1,3] Christina Xu,[1] Lukas Kater,[2] Georg Kempf,[2] Brenda Martínez-González,[1] David Akopian,[1,8] Stephanie K. See,[4,9] Nicolas H. Thomä,[2,*] and Michael Rapé[1,3,5,10,*]

[1]Department of Molecular and Cell Biology, University of California at Berkeley, Berkeley, CA, USA
[2]Friedrich Miescher Institute for Biomedical Research, Basel, Switzerland
[3]Howard Hughes Medical Institute, University of California at Berkeley, Berkeley, CA, USA
[4]Center for Emerging and Neglected Diseases, University of California at Berkeley, Berkeley, CA 94720, USA
[5]California Institute for Quantitative Biosciences (QB3), University of California at Berkeley, Berkeley, CA 94720, USA
[6]These authors contributed equally
[7]These authors contributed equally
[8]Present address: Nutcracker Therapeutics, Emeryville, CA, USA
[9]Present address: Insitro, South San Francisco, CA, USA
[10]Lead contact
*Correspondence: nicolas.thoma@fmi.ch (N.H.T.), mrape@berkeley.edu (M.R.)
https://doi.org/10.1016/j.cell.2023.06.015

SUMMARY

All eukaryotes require intricate protein networks to translate developmental signals into accurate cell fate decisions. Mutations that disturb interactions between network components often result in disease, but how the composition and dynamics of complex networks are established remains poorly understood. Here, we identify the E3 ligase UBR5 as a signaling hub that helps degrade unpaired subunits of multiple transcriptional regulators that act within a network centered on the c-Myc oncoprotein. Biochemical and structural analyses show that UBR5 binds motifs that only become available upon complex dissociation. By rapidly turning over unpaired transcription factor subunits, UBR5 establishes dynamic interactions between transcriptional regulators that allow cells to effectively execute gene expression while remaining receptive to environmental signals. We conclude that orphan quality control plays an essential role in establishing dynamic protein networks, which may explain the conserved need for protein degradation during transcription and offers opportunities to modulate gene expression in disease.

INTRODUCTION

Metazoan development depends on the formation of protein complexes that differ widely in their stability, stoichiometry, and composition.[1–3] Although interactions between enzymes and substrates may persist only for seconds,[4] large complexes such as the nuclear pore exist for years.[5] When the same complex contains both stable and rapidly exchanging subunits, it is often the transiently bound component that provides important points of regulation.[3,6]

Cells use multiple mechanisms to establish interactions at different time scales. Persistent binding is often based on the complementary recognition of amino acid side chains or hydrophobic surfaces of folded domains.[7,8] By contrast, dynamic complexes can rely on intrinsically disordered regions (IDRs) that engage their partners with weak affinity but gain avidity through multivalent binding to several proteins at a time.[9,10] Interactions are further modulated by posttranslational modifications, including phosphorylation or ubiquitylation,[11,12] or small hormones and metal ions that mediate substrate recognition by E3 ligases.[13,14] Developmental signaling requires that all types of interactions are integrated into a coherent response, but how this is accomplished is not well understood.

Accurate complex formation is particularly important for the transcriptional programs that specify cell fate. To find their targets in chromatin, many transcription factors dimerize through zinc fingers, BTB domains, or leucine zippers.[15,16] As shown for the pluripotency factors OCT4 and SOX2, dimerization can occur during the search for target motifs, and the complex falls apart when OCT4 and SOX2 dissociate from DNA.[17] Transcription factors of the BTB family use an alternative strategy and co-translationally form homodimers that are stable for days.[18,19] As aberrant heterodimerization impedes BTB function, cells evolved dimerization quality control to eliminate mispaired transcription factors and, thereby, ensure nervous system development.[1,18,20]

In addition to dimerization motifs, transcription factors contain activation domains that are rich in IDRs.[21–23] A multiplicity of

binding sites within IDRs allows gene expression regulators to engage many proteins at a time and nucleate networks referred to as transcription factories, hubs, or condensates.[16,24–26] Transcription hubs enrich components of the gene expression machinery by up to 1,000-fold over nucleoplasmic levels,[27] which improves the ability of c-Myc, OCT4, or the oncogenic EWS-FLI1 to stimulate gene expression.[21,28,29] Despite high protein concentrations, transcription hubs can be rapidly remodeled in response to changing cellular needs,[26] yet subtle increases in protein levels or reduced network dynamics can disturb gene expression and cause disease.[28,30,31] How cells establish the composition and dynamics of transcription hubs, or more generally protein networks, is not well known.

Here, we report that cells use orphan quality control to create dynamic protein interaction networks driving gene expression. Crucial to this regulation is the E3 ligase UBR5, which helps degrade orphan subunits of multiple transcriptional factors that function within a network centered on the c-Myc oncoprotein. By eliminating unpaired transcription factors, UBR5 establishes dynamic interactions that allow cells to effectively execute gene expression while remaining responsive to changes in their environment. Orphan quality control, therefore, plays a crucial regulatory role in creating protein networks that can faithfully transmit changes in cell state to the transcriptional machinery defining cell fate.

RESULTS

UBR5 binds multiple transcriptional regulators

We had recently identified UBR5 as a regulator of hESC self-renewal.[32] Intriguingly, inactivating mutations in *UBR5* drive mantle cell lymphoma,[33] whereas breast or ovarian cancers amplify *UBR5* to support tumor growth and metastasis.[34–36] How an E3 ligase can both regulate stem cell identity and act as either a tumor suppressor or an oncogene was unknown.

To address this question, we appended FLAG epitopes to the *UBR5* loci in 293T and HeLa cells and isolated endogenous interactors by affinity purification and mass spectrometry.[2,37] UBR5 bound subunits of the INO80 complex that sustains open chromatin at pluripotency enhancers[38–40] (Figure 1A), and it engaged SPT4 and SPT5, which bind each other and control transcript elongation in stem cells.[41–44] UBR5 also associated with the mitotic checkpoint complex (MCC), PLK1 kinase, and the kinesin KIF2A. PLK1 and MCC regulate the anaphase-promoting complex (APC/C), which controls nucleosome occupancy at transcription start sites of pluripotency genes.[32]

Affinity purification and western blotting confirmed the association of UBR5 with subunits of INO80, including MCRS1, and components of the MCC, as well as SPT4, SPT5, and KIF2A (Figure 1B). KIF2A depletion did not affect UBR5 recognition of MCC or SPT5, and a reduction in MCC or SPT5 did not impact KIF2A binding to UBR5 (Figures 1C and 1D; Figure S1A); these proteins bind UBR5 independently of each other. However, the loss of BUBR1 and BUB1 diminished the interaction with other MCC subunits, and the depletion of SPT5 destabilized SPT4 and reduced its binding to UBR5 (Figure 1D; Figure S1A). To assess whether UBR5 engages these proteins in complexes, we performed sequential affinity purification of UBR5 and SPT5. Although UBR5 stably bound SPT5, the second immunoprecipitation did not enrich for SPT4 and, therefore, revealed that UBR5 can engage SPT5 independently of its partner SPT4 (Figure 1E). Using specific antibodies, we found that UBR5 formed similar interactions in human embryonic stem cells (hESCs) (Figure 1F).

Intriguingly, INO80, APC/C, and KIF2A all engage WDR5,[32,39,45] a methylhistone reader that recruits c-Myc to chromatin.[46] SPT5 and the INO80 component MCRS1 bind c-Myc and N-Myc, respectively.[44,47] In addition, PLK1 affects c-Myc stability and function,[48] and UBR5 is co-amplified with c-Myc in cancer and was proposed to target c-Myc for degradation.[34,49] Indeed, we found that UBR5 binds to c-Myc (Figure 1B). UBR5, therefore, engages many proteins within a network centered on c-Myc (Figure 1G), a transcription factor that helps establish stem cell identity and is frequently mutated in cancer.[50,51]

UBR5 degrades transcriptional regulators

UBR5 produces branched ubiquitin chains that elicit efficient proteasomal degradation.[52–54] To test whether UBR5 triggers transcription factor degradation, we fused its interactors and related proteins to GFP and co-expressed them with mCherry under the control of an internal ribosome entry site. The ratio between GFP and mCherry, as measured by flow cytometry, reports on the stability of the GFP-tagged protein.[55–57] UBR5 substrates should display a higher GFP to mCherry ratio upon the depletion of the E3 ligase by siRNAs.

This screen revealed 21 potential targets of UBR5 (Figure 2A; Figure S1B). In addition to c-Myc,[34,49] UBR5 depletion stabilized the SPT4 and SPT5 regulators of transcript elongation, INO80 components (INO80B, INO80C, INO80F, MCRS1, and RUVBL2), and the MCC subunit CDC20. UBR5 was also needed for the degradation of transcription factors and transcriptional regulators that cooperate with c-Myc and control cell fate, such as OCT4, MAFF, NFIL3, NRL, SMARCB1, and TAF1A, or are activated by stress, including ATF3 and CHOP.

The deletion of *UBR5* in two cell lines confirmed that these transcription factors were stabilized by E3 ligase inactivation (Figure 2B; Figure S1C). We made similar observations upon deletion of the endogenous HECT (homologous to E6-AP C-terminus) or UBA (ubiquitin associated) domains of UBR5, which reduced UBR5 levels and protected transcription factors from degradation (Figure 2B; Figure S2A). As expected for a HECT family E3 ligase, UBR5 required the ubiquitin-activating E1 enzyme UBA1 and the Cys-specific ubiquitin-conjugating E2 enzyme UBE2L3 for efficient degradation (Figure 2C; Figures S2B and S2C). UBR5 substrates were also turned over in a p97- and proteasome-dependent manner, whereas the lysosome was not required (Figures 2D and 2E; Figures S2D–S2F). Importantly, the abundance of several endogenous transcription factors increased in dividing cells that lacked *UBR5* or carried deletions of its HECT or UBA domains (Figure 2F; Figure S2A).

As a further test for specificity, we depleted E3 ligases that were structurally or functionally related to UBR5. Apart from SPT4 and SMARCB1, which were also stabilized by loss of the UBR4 or CHIP, each candidate substrate was most strongly protected from degradation by UBR5 depletion (Figure 2G). We finally repeated the entire screen in HUWE1-depleted cells and found that this E3 ligase targets distinct substrates (Figure S2G).

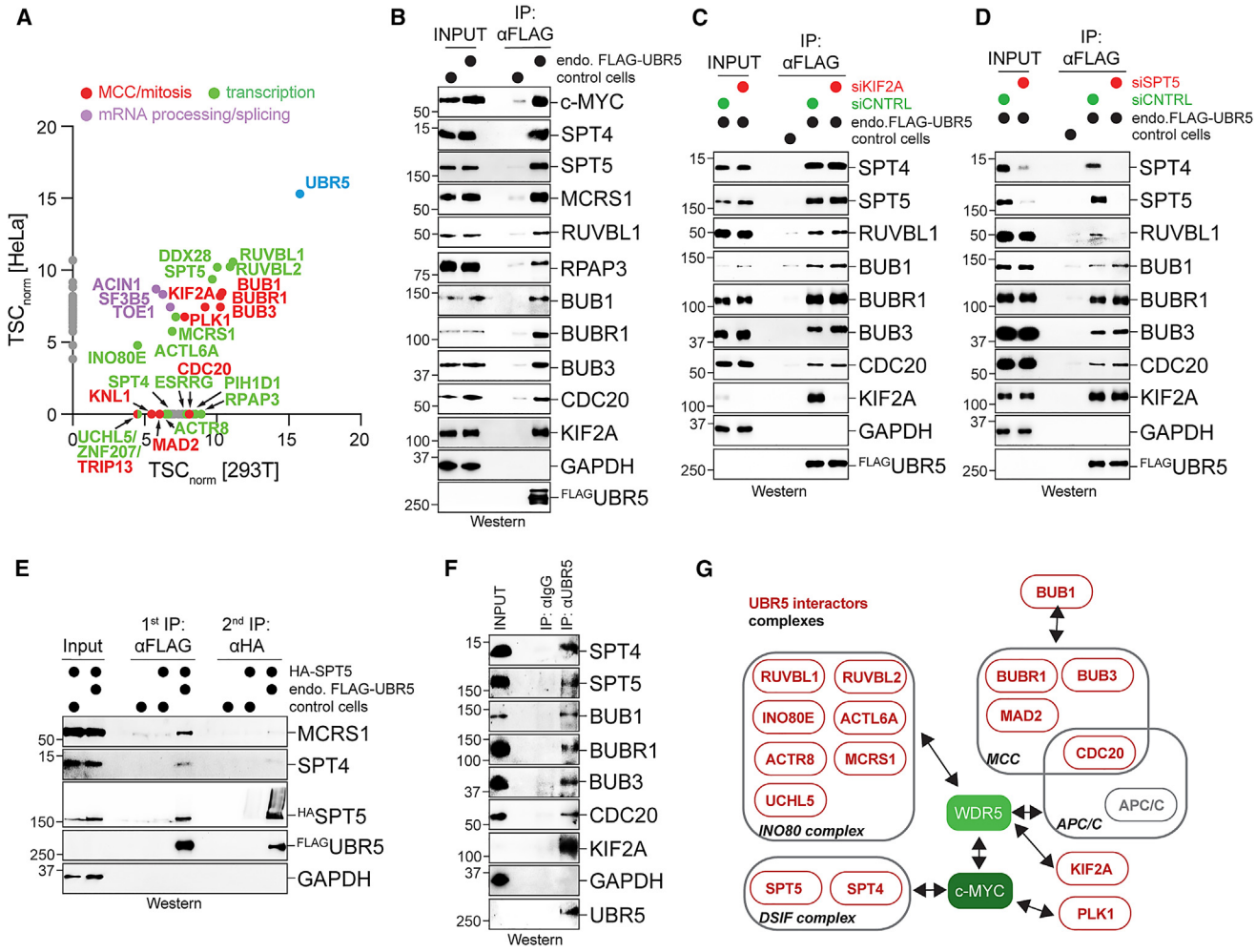

Figure 1. UBR5 binds transcriptional regulators with connections to c-Myc

(A) Identification of endogenous ^{FLAG}UBR5 partners from 293T and HeLa cells by affinity purification and mass spectrometry.

(B) Validation of UBR5 interactors in HeLa cells by affinity purification and western blot analysis.

(C) Depletion of KIF2A only reduces this protein in ^{FLAG}UBR5 affinity purifications from HeLa cells.

(D) Depletion of SPT5 destabilizes and reduces UBR5 binding of SPT4 in HeLa cells.

(E) Endogenous ^{FLAG}UBR5 was immunoprecipitated from HeLa cells expressing ^{HA}SPT5. Eluates were purified on αHA-resin and probed for UBR5, SPT4, and MCRS1 by western blot analysis.

(F) Endogenous UBR5 was precipitated from hESC lysate using specific antibodies and probed for co-purifying proteins by western blot analysis.

(G) Most UBR5 partners have close links to the c-Myc/WDR5 complex.

See also Figure S1.

Together, these results reveal a role for UBR5 in degrading transcription factors that have close links to c-Myc, are frequently misregulated in cancer, and are required for maintaining stem cell pluripotency.

UBR5 ubiquitylates transcription factors

We next asked whether UBR5 directly modifies its targets with proteolytic ubiquitin chains. Indeed, endogenous UBR5 ubiquitylated most degradation targets, including the INO80 components MCRS1, INO80C, and RUVBL2; the transcription factors c-Myc and NFIL3; the regulator of transcription elongation SPT5; and CDC20 (Figure 3A; Figure S3A). UBR5 cooperated with either UBE2D3 or the Cys-specific E2 UBE2L3 (Figures 3A and 3B; Figure S3B) but failed to ubiquitylate SPT4 and several proteins that it did not turn over in cells (Figure S3C). The ability of UBR5 to modify its target MCRS1 required an active HECT domain and the UBA domain (Figure 3C), although the latter may also play structural roles (Figure S3D).

Ubiquitin variants revealed that UBR5 showed a strong preference for K48 linkages, but when reticulocyte lysate was used to synthesize substrates, chain formation was also reduced if the K63 of ubiquitin was mutated (Figure 3D). Ubiquitylation was enhanced if MCRS1 was fused to ubiquitin (Figure 3E; Figure S3E), and pre-ubiquitylated MCRS1 was modified in a more K48-specific manner (Figure 3E). These observations suggested that UBR5 assembles heterotypic chains that are

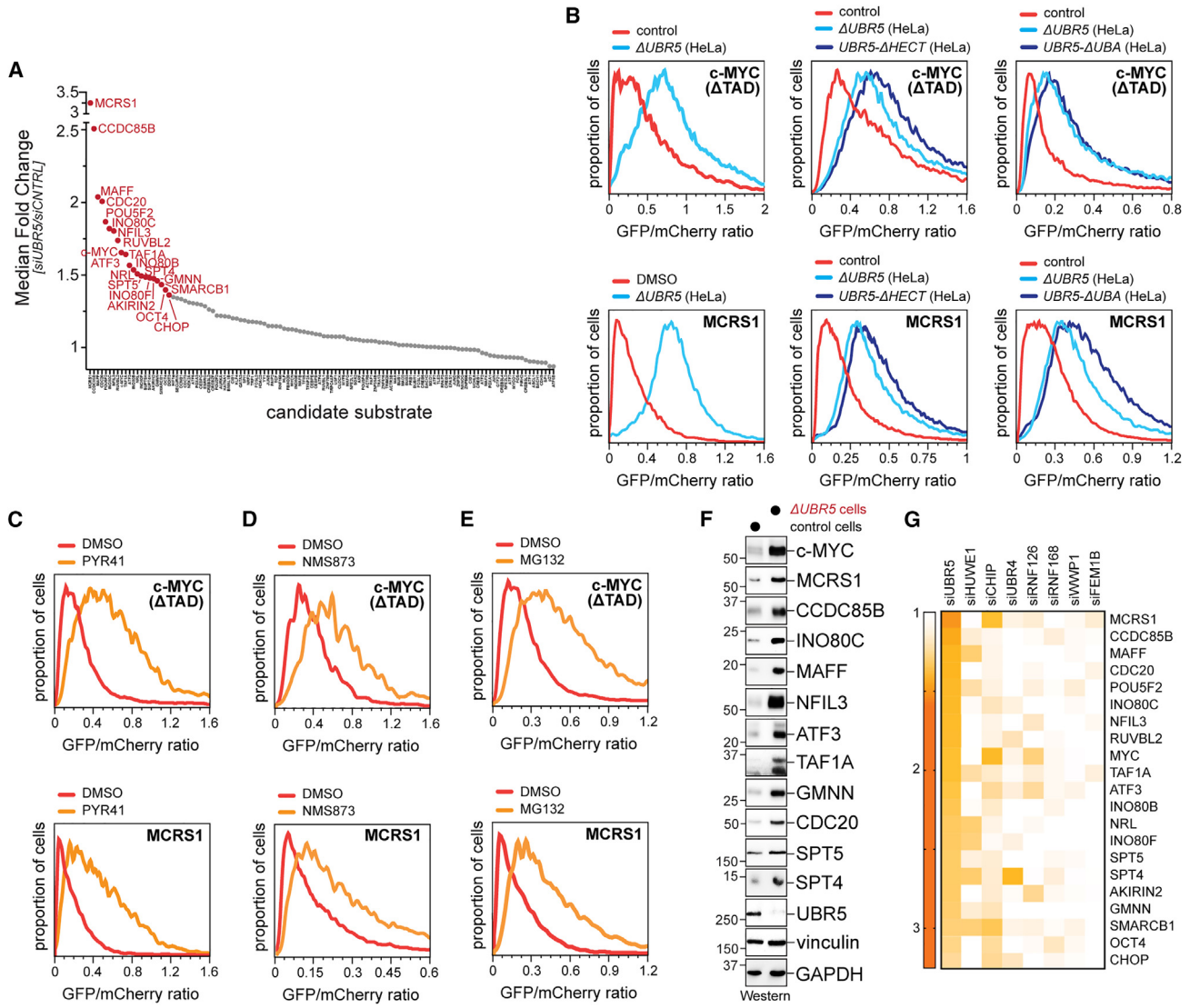

Figure 2. UBR5 degrades transcriptional regulators with connections to c-Myc

(A) A flow-cytometry-based screen identifies candidate UBR5 substrates in HeLa cells.

(B) Validation of the c-Myc$^{\Delta TAD}$ and MCRS1 targets in *ΔUBR5* HeLa cells or cells with the deletion of the UBR5 HECT or UBA domain (blue: genetic manipulation; orange: chemical manipulation).

(C) UBR5 targets are stabilized upon E1 enzyme inhibition with PYR41.

(D) UBR5 targets are stabilized upon p97 inhibition with NMS873.

(E) UBR5 targets are stabilized upon proteasome inhibition.

(F) Endogenous UBR5 targets increase in *ΔUBR5* HeLa cells, as determined by western blot analysis.

(G) Stability of UBR5 substrates was determined in cells depleted of related E3 ligases.

See also Figures S1 and S2.

dominated by K48 linkages and known to be recognized by p97, and ubiquitylated MCRS1 was indeed captured by p97 (Figure S3F). We conclude that UBR5 directly acts on transcriptional regulators to induce their p97- and proteasome-dependent degradation.

UBR5 is required for accurate gene expression

To determine how transcription factor degradation impacts gene expression, we performed RNA-seq in *ΔUBR5* 293T cells and hESCs that were acutely depleted of UBR5. We found that the lack of UBR5 upregulated some genes that included targets of c-Myc (Figure 4A; Figure S4A). We confirmed these results by qRT-PCR (Figure 4B). Many genes that were expressed more efficiently in *ΔUBR5* cells were long transcripts that are normally expressed at low levels (Figure S4B), and they included *CCND1*, a major driver of the mantle cell lymphoma that is caused by *UBR5* inactivation.[58] UBR5 deletion had little effect on c-Myc expression itself (Figure S4C).

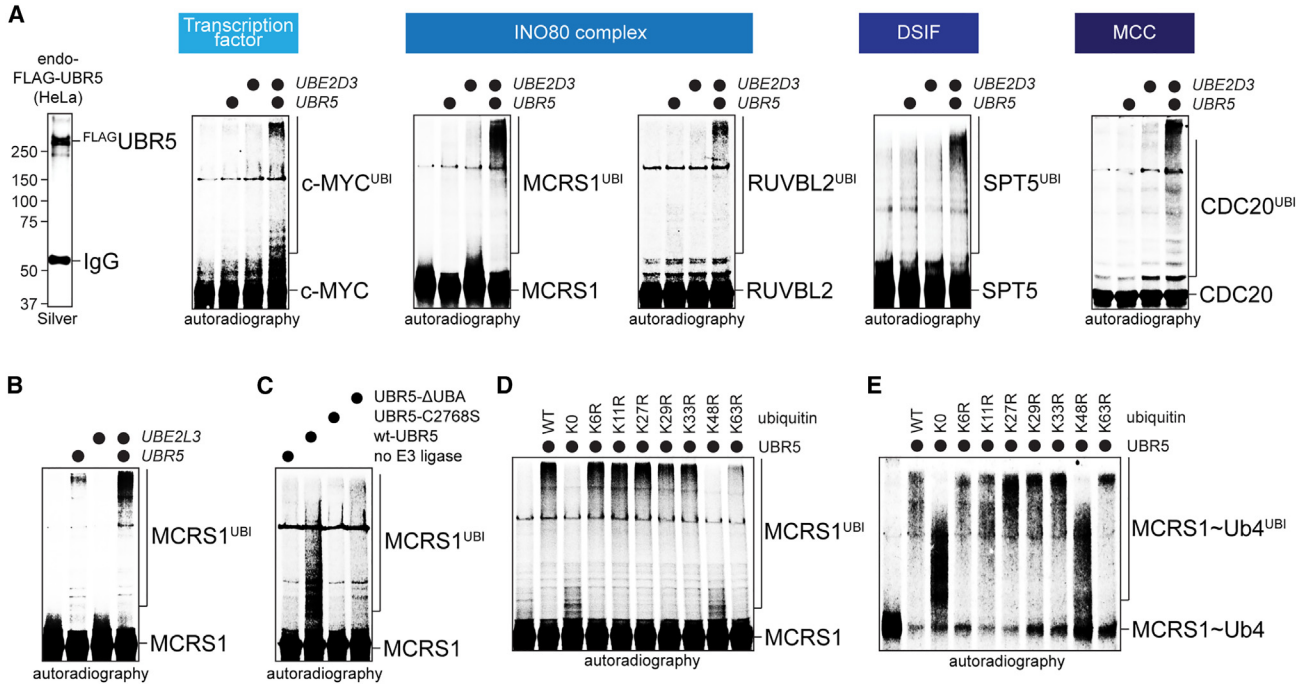

Figure 3. UBR5 ubiquitylates transcriptional regulators

(A) Endogenous UBR5 was purified from HeLa cells and incubated with E1, UBE2D3, ubiquitin, and ^{35}S-labeled targets produced by in vitro transcription/translation (IVT/T). Substrate modification was analyzed by autoradiography (left panel: a silver-stained gel of UBR5).

(B) ^{35}S-labeled MCRS1 was incubated with UBR5, E1, UBE2L3, and ubiquitin.

(C) UBR5, UBR5^{C2768S}, and UBR5$^{\Delta UBA}$ were incubated with ^{35}S-labeled MCRS1.

(D) ^{35}S-labeled MCRS1 was incubated with UBR5, E1, UBE2D3, and ubiquitin mutants and analyzed for ubiquitylation as above.

(E) ^{35}S-labeled MCRS1-Ub$_4$ was incubated with UBR5, E1, UBE2D3, and ubiquitin mutants.

See also Figure S3.

Surprisingly, UBR5 deletion reduced the expression of even more c-Myc targets (Figure 4A). Having validated impaired gene expression by qRT-PCR (Figure 4C), we found that those genes predominantly encoded short transcripts that might be initiated more often (Figure 4D). Similar genes were downregulated in *ΔUBR5* HeLa cells or cells with the endogenous deletion of the HECT or UBA domain of UBR5 (Figure 4E). Although UBR5 degrades transcription factors, it supports, rather than restricts, the expression of several c-Myc targets.

To determine whether UBR5 substrates were required for this regulation, we depleted c-Myc, MCRS1, or other targets and measured gene expression by qRT-PCR. Depleting these transcription factors diminished the mRNA levels of UBR5-dependent genes and dampened the effects of *UBR5* loss on upregulated genes (Figures 4F and 4G; Figures S4D and S4E). Moreover, their depletion phenotypes correlated with each other and with UBR5 in DepMap (Figure S4F). Thus, UBR5-dependent degradation sustains gene expression driven by multiple transcription factors that act within a network centered on the c-Myc oncoprotein.

UBR5 targets unpaired c-Myc molecules

How could transcription factor degradation support gene expression? To address this question, we asked how UBR5 recognizes c-Myc and first found that it targets c-Myc independently of the phosphodegron detected by its established E3 ligase SCF^{FBXW7} (Figure S5A). Although deletion of the entire transactivation domain of c-Myc did not prevent UBR5-mediated turnover (Figures 5A and 5B), the carboxy-terminal domain with its helix-loop-helix and leucine zipper motifs was necessary and sufficient for turnover by UBR5 (Figure 5C; Figure S5B). As UBR5 is nuclear (Figure S5C), this c-Myc domain was only targeted by UBR5 if fused to a nuclear import signal, and a different enzyme mediated its turnover in the cytoplasm (Figure S5D).

By performing Ala and Glu scans of the carboxy-terminal domain, we identified motifs in the basic region and leucine zipper that each supported UBR5-dependent degradation (Figures 5D and 5E; Figure S5E). We noted similar motifs in N-Myc and other UBR5-targets (Figure 5F), which is consistent with N-Myc being degraded through UBR5 (Figure S5F). TAMRA-labeled peptides of candidate degrons were efficiently ubiquitylated by UBR5 (Figure 5G), which relied on K48 of ubiquitin and Cys2768 in its HECT domain for chain formation (Figures 5H and 5I). We conclude that c-Myc contains two degrons in its basic region and leucine zipper domain that are each sufficient to mediate recognition by UBR5.

Mapping these degrons on the structure of c-Myc/MAX complexes[59] showed that both motifs are buried when c-Myc binds MAX and engages DNA (Figure 5J). Indeed, the mutation of its degrons disrupted the interaction of c-Myc with MAX (Figure 5E), which implied that c-Myc can bind either MAX or UBR5, but not

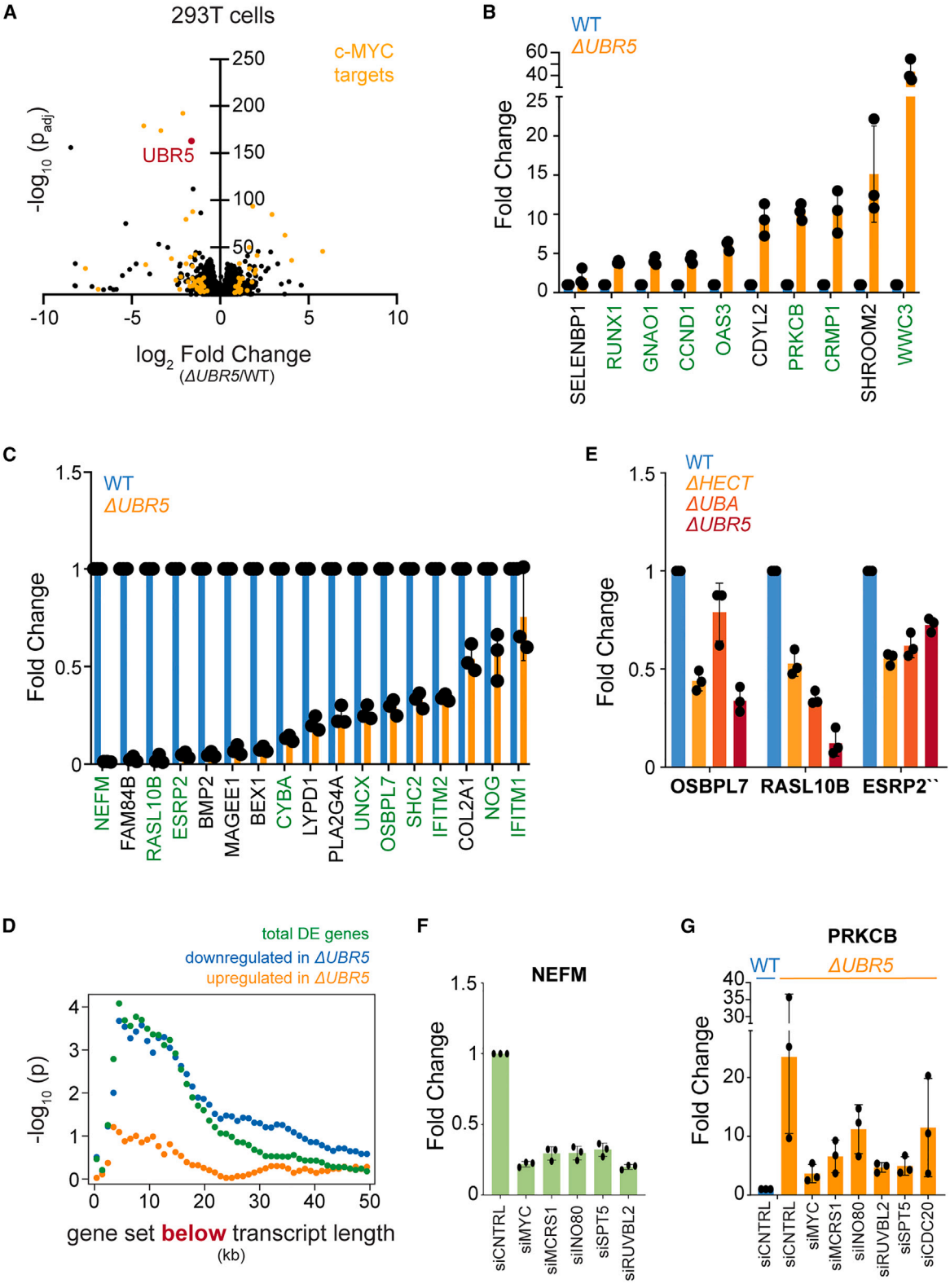

(legend on next page)

both. MAX overexpression accordingly prevented c-Myc degradation through UBR5 (Figures 5E and 5K; Figure S5G), although MAX was not targeted by UBR5 and, therefore, did not simply compete with c-Myc for access to UBR5 (Figure S5H). The depletion of MAX had the opposite effect and stimulated the capture of c-Myc by UBR5 (Figure 5L) and the degradation of c-Myc through UBR5 and p97 (Figure 5M; Figure S5I). Thus, UBR5 targets c-Myc molecules that are not bound to MAX or DNA. Notably, we found by RNA-seq and ribosome profiling that hESCs produce c-Myc in large excess over MAX (Figure 5N), suggesting that cells compensate for c-Myc degradation by re-synthesizing the continuously degraded transcription factor. We conclude that UBR5 selectively targets unpaired c-Myc molecules (Figure 5O).

UBR5 performs orphan quality control

As a c-Myc peptide inhibited the ubiquitylation of MCRS1 and SPT5 (Figure S6A), UBR5 recognizes these transcription factors through a common site. Accordingly, MCRS1 and SPT5 possess motifs that resemble the first c-Myc degron (Figure 5F) and were ubiquitylated by UBR5 (Figures 6A and 6B). The modification of the SPT5 degron was dependent on the catalytic Cys, but not the UBA domain of UBR5 (Figure 6C). While the MCRS1 degron is in its FHA domain, a known interaction module,[60] the SPT5 degron overlaps with its DNA-binding region.[61] UBR5 might, therefore, also modify other targets when they are not engaged with DNA or protein partners.

Consistent with this hypothesis, the co-expression of binding partners stabilized each UBR5 substrate: MAFF and CDC20 were protected by their interactors BACH2 and MCC to the same extent as by UBR5 depletion (Figure 6D; Figure S6B); for such targets, UBR5 is the main orphan E3 ligase. MCRS1, RUVBL2, and OCT4 were stabilized by the co-expression of their partners or UBR5 depletion, yet partners stabilized the target to a larger extent than the loss of UBR5 (Figures 6E–6G); these proteins are controlled as orphans by both UBR5 and other E3s. By contrast, SPT4 was much more stabilized by the co-expression of SPT5 than by the loss of UBR5 (Figure S6C). Consistent with the failure of UBR5 to ubiquitylate SPT4 (Figure S3C), SPT4 relies on other E3 ligases for turnover. As with c-Myc, the deletion of the degron-containing FHA domain in MCRS1 diminished binding to both UBR5 and its stabilizing partners (Figure S6D), and hESCs produce the UBR5 substrates MCRS1, OCT4, SPT5, and MAFF in large excess over stabilizing partners (Figure S6E). Similar to MAX, most stabilizers were not degraded through UBR5 (Figure S6F).

Endogenous MAFF was also turned over upon loss of its partner BACH2 but stabilized by UBR5 co-depletion (Figure 6H), and OCT4 disappeared in hESCs in a UBR5-dependent manner if SOX2 had been depleted (Figure 6I). Substrate behavior was independent of how we removed UBR5: akin to siRNA depletion, *UBR5* deletion by genome editing rescued the drop in SPT5 upon the loss of SPT4 (Figure 6J). In line with other enzymes acting on SPT4 (Figure S3C), *UBR5* deletion did not stabilize SPT4 in the absence of SPT5 (Figure S6G). UBR5, therefore, targets multiple transcriptional regulators within the c-Myc network as orphan proteins.

Structure of substrate-bound UBR5

To decipher how UBR5 gains substrate specificity, we analyzed its binding to recombinant MCRS1. AlphaFold2 predictions highlighted the carboxy-terminal forkhead-associated (FHA) domain in MCRS1 (Figure 6K), which was required for efficient recognition by UBR5 (Figure S6H). When mapping corresponding domains in UBR5, we found that its HECT domain was sufficient to engage MCRS1 (Figure S6I). In support of our degron analyses, these studies suggested that the FHA domain of MCRS1 is recognized by the HECT domain of UBR5.

We then purified the UBR5-MCRS1 complex and used cryo-EM to obtain a density map with an overall resolution of 4.4 Å (Figure 6L; Figure S7). As seen for the apo-UBR5 structure,[62–64] UBR5 forms a tetramer with four HECT domains pointing toward the center of an E3 ligase ring, and this architecture was largely unchanged in substrate-bound UBR5. Importantly, we observed additional density in the presence of MCRS1 near the C-lobe of the UBR5 HECT domain, which allowed rigid body docking of an AlphaFold2 model of MCRS1's FHA domain. The remainder of MCRS1 was not visible and hence likely adopts multiple conformations.

Although the local resolution of the FHA domain at ~8 Å in principle allows multiple docking poses, crosslink mass spectrometry indicated a preferred orientation (Figure S6J). A high-scoring reproducible crosslink occurred between K397 in MCRS1 and K2786 in the C-lobe of UBR5, which positions the MCRS1 degron in an orientation close to the catalytic Cys of UBR5 primed for ubiquitylation (Figure 6M). This places the FHA domain of MCRS1 between the HECT domain of one UBR5 and the tandem domain of another subunit and thus greatly limits its ability to bind other proteins (Figure 6M). Substrate sandwiching by distinct subunits of tetrameric UBR5 could, therefore, explain why UBR5 selectively ubiquitylates unpaired MCRS1 molecules and thus acts as an orphan E3 ligase.

Orphan transcription factor degradation establishes network dynamics

Orphan degradation is thought to provide quality control for unpaired proteins that emerge due to an unbalanced synthesis of

Figure 4. UBR5 is required for accurate gene expression

(A) RNA-seq analysis shows aberrant gene expression in *ΔUBR5* 293T cells (yellow: c-Myc target genes).

(B) Confirmation of upregulated genes in *ΔUBR5* cells by qRT-PCR (green: c-Myc target genes). Data are represented as mean ± SD.

(C) Confirmation of downregulated genes in *ΔUBR5* cells by qRT-PCR (green: c-Myc target genes). Data are represented as mean ± SD.

(D) UBR5-dependent genes encode short transcripts, as shown by the likelihood that genes below a certain transcript length are reduced in the absence of *UBR5*.

(E) Similar genes are downregulated in *ΔUBR5* HeLa cells and cells lacking endogenous HECT or UBA domain of UBR5. Data are represented as mean ± SD.

(F) Depletion of UBR5 substrates reduces the expression of UBR5-dependent genes. Data are represented as mean ± SD.

(G) Depletion of UBR5 substrates blunts the expression of genes upregulated upon *UBR5* deletion. Data are represented as mean ± SD.

See also Figure S4.

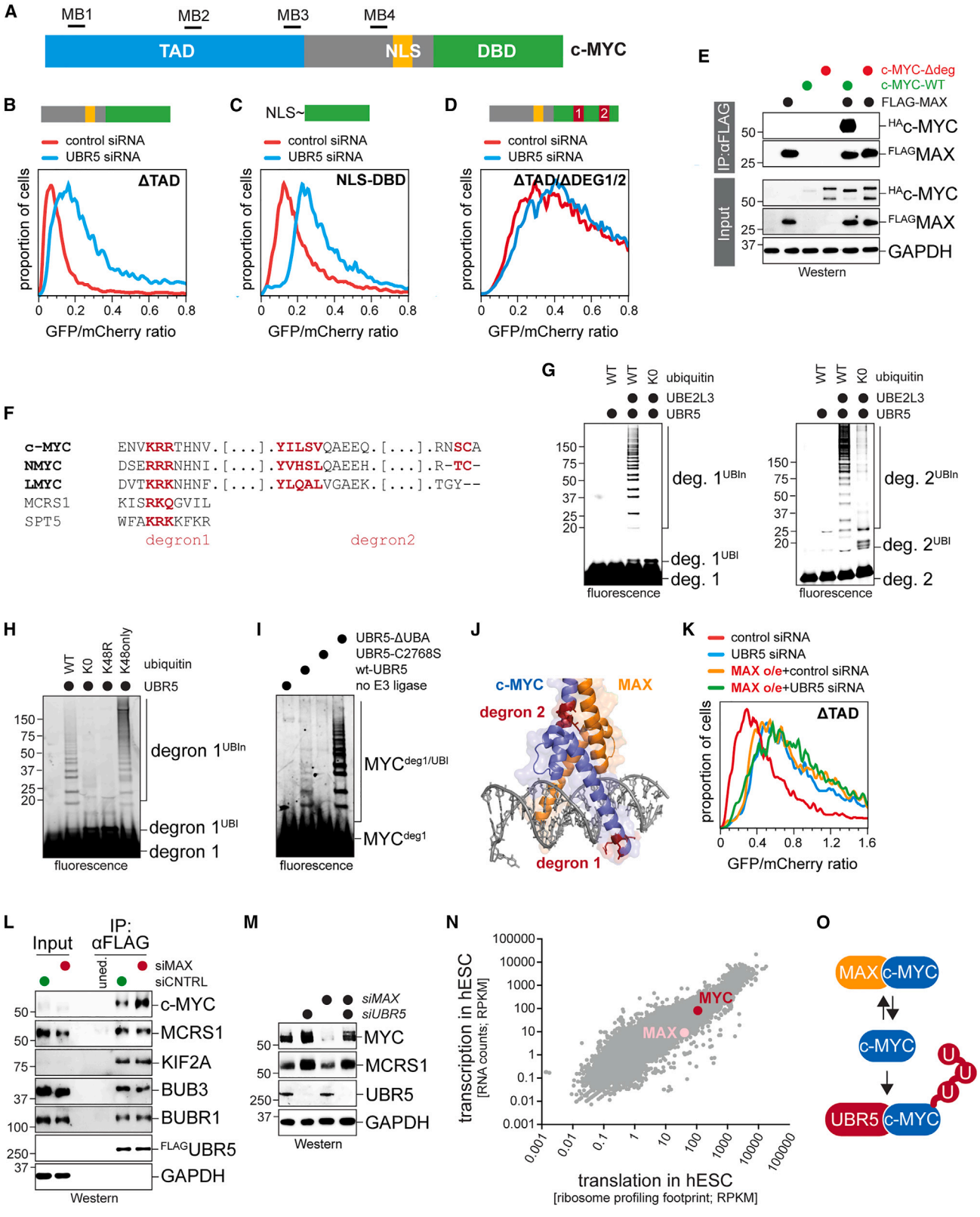

(legend on next page)

complex components or as a result of stresses that alter the efficiency or kinetics of interactions.[65] If UBR5 siphons away such aberrant subunits, potentially to prevent their aggregation, its loss should increase its targets, but not active complexes. By contrast, if orphans are formed as a normal step during gene expression, UBR5 deletion might alter the abundance or dynamics of transcription factor complexes.

Consistent with the latter hypothesis, we found that the loss of UBR5 strongly increased the interaction between c-Myc and ^{FLAG}MAX (Figure 7A). A similar increase in complex formation was seen for endogenous c-Myc and MAX in *ΔUBR5* cells (Figure 7B). The effects of *UBR5* deletion were even more drastic if c-Myc was overexpressed, as expected for a condition that produces more unpaired c-Myc (Figure S8A). UBR5, therefore, targets c-Myc molecules that can dimerize with MAX and, hence, are at least partially functional.

UBR5 could eliminate nascent c-Myc or molecules that were released from c-Myc/MAX complexes. To distinguish between these possibilities, we expressed c-Myc^{T58A}, which is not recognized by SCF^{FBXW7} and forms more abundant complexes with MAX,[66] and then treated cells with the translation inhibitor cycloheximide to prevent c-Myc synthesis. Importantly, c-Myc^{T58A}/MAX complexes rapidly disappeared upon cycloheximide treatment, and this response was strongly delayed in *ΔUBR5* cells (Figure 7C). Although wild-type c-Myc formed fewer complexes, *UBR5* deletion also prolonged their persistence (Figures S8A and S8B). c-Myc/MAX complexes similarly disappeared in a UBR5-dependent manner if we inhibited protein synthesis by the activation of the integrated stress response (Figure 7D), and this reduced the expression of select UBR5-dependent genes (Figure S8C). These experiments show that c-Myc/MAX complexes are frequently dismantled, and UBR5 targets dissociated c-Myc molecules for degradation.

Suggesting that a similar regulation occurs beyond c-Myc, complexes between MCRS1 and its stabilizer CCDC85B disappeared after cycloheximide treatment yet persisted much longer in *ΔUBR5* cells (Figure 7E; Figure S8D). The loss of *UBR5* also retained c-Myc bound to MCRS1, suggesting that UBR5 restricts broader interactions within the network. The deletion of MCRS1's FHA domain prevented the interaction between MCRS1 and c-Myc (Figure S6D), which documents that network interactions required the same domain that is regulated by orphan degradation. The changes in interaction dynamics impacted which partners MCRS1 engages: although MCRS1 normally bound SPT5, which functions in transcript elongation, it failed to associate with this protein in *ΔUBR5* (Figure 7F). By contrast, MCRS1 still interacted in *ΔUBR5* cells with INO80, which acts early in transcription by modulating chromatin architecture. This behavior mirrors c-Myc, which fails to hand the regulators of transcription elongation over to RNA polymerase II if its ubiquitylation is impaired.[67,68] Orphan degradation thus allows transcriptional programs to execute successive steps while remaining receptive to changes in the cellular environment.

DISCUSSION

Quality control pathways are often thought to eliminate defective proteins to prevent aggregation and tissue degeneration. As the propensity for protein misfolding increases with age, the phenotypes of impaired quality control are frequently observed after the reproductive phase,[69–73] and why these systems have been conserved so well through evolution is not fully understood. Here, we show that stem cells use orphan quality control to establish dynamic interactions between transcription factors that preserve pluripotency. The loss of the central E3 ligase, UBR5, stabilizes transcription factor complexes and, thereby, compromises the efficiency and adaptability of gene expression. Our findings reveal a regulatory role of quality control beyond the removal of toxic proteins, which may explain the conserved need for degradation in gene expression and offers exciting possibilities to modulate the transcription machinery for therapeutic benefit.

UBR5 exerts orphan quality control

We previously identified UBR5 as a regulator of hESC self-renewal,[32] but how this E3 ligase acts at the interface of development and disease was unclear. We now show that UBR5 helps degrade multiple transcriptional regulators that act within a network centered on the c-Myc oncoprotein and are essential

Figure 5. UBR5 targets orphan c-Myc

(A) Scheme of c-Myc, including transactivation domain (TAD), nuclear localization signal (NLS), and DNA-binding domain (DBD).
(B) Levels of c-Myc$^{\Delta TAD}$-GFP::mCherry reporters were analyzed in cells treated with control or UBR5-siRNAs by flow cytometry.
(C) The carboxy-terminal domain of c-Myc, when fused to an NLS, is sufficient to mediate UBR5-dependent degradation.
(D) Mutations in the basic helix-loop-helix and leucine zipper motifs protect c-Myc from UBR5-dependent degradation.
(E) Degron motifs were mutated in ^{HA}c-Myc and variants expressed alone or in the presence of ^{FLAG}MAX. Where indicated, ^{FLAG}MAX was immunoprecipitated, and co-purifying c-Myc detected by western blot analysis.
(F) Degron motifs in c-Myc, N-Myc, L-Myc, SPT5, and MCRS1. Mutated residues in the c-Myc degrons are shown in red.
(G) TAMRA-labeled c-Myc degrons were incubated with E1, UBE2L3, UBR5, and ubiquitin, and ubiquitylation was detected by fluorescence.
(H) Modification of TAMRA-labeled degron 1 peptide with UBR5 and either lysine-free ubiquitin (K0), K48R ubiquitin, or ubiquitin with K48 as its only Lys (K48only).
(I) UBR5, UBR5^{C2768S}, and UBR5$^{\Delta UBA}$ were assessed for their ability to ubiquitylate the c-Myc degron 1.
(J) Structural model of the c-Myc/MAX complex, showing that degrons (red) are shielded by DNA binding and heterodimerization.
(K) MAX overexpression stabilizes c-Myc to the same extent as UBR5 depletion.
(L) Depletion of MAX increases the binding of c-Myc, but not other proteins, to UBR5. Endogenous ^{FLAG}UBR5 was immunoprecipitated from 293T cells treated with proteasome inhibitors, and co-purifying proteins were detected by western blot analysis.
(M) Cells were treated with control, MAX, or UBR5 siRNAs, and the levels of c-Myc were determined by western blot analysis.
(N) hESCs transcribe and translate c-Myc in large excess over MAX, as shown by RNA-seq and ribosome profiling.
(O) Model of orphan c-Myc degradation by UBR5.
See also Figure S5.

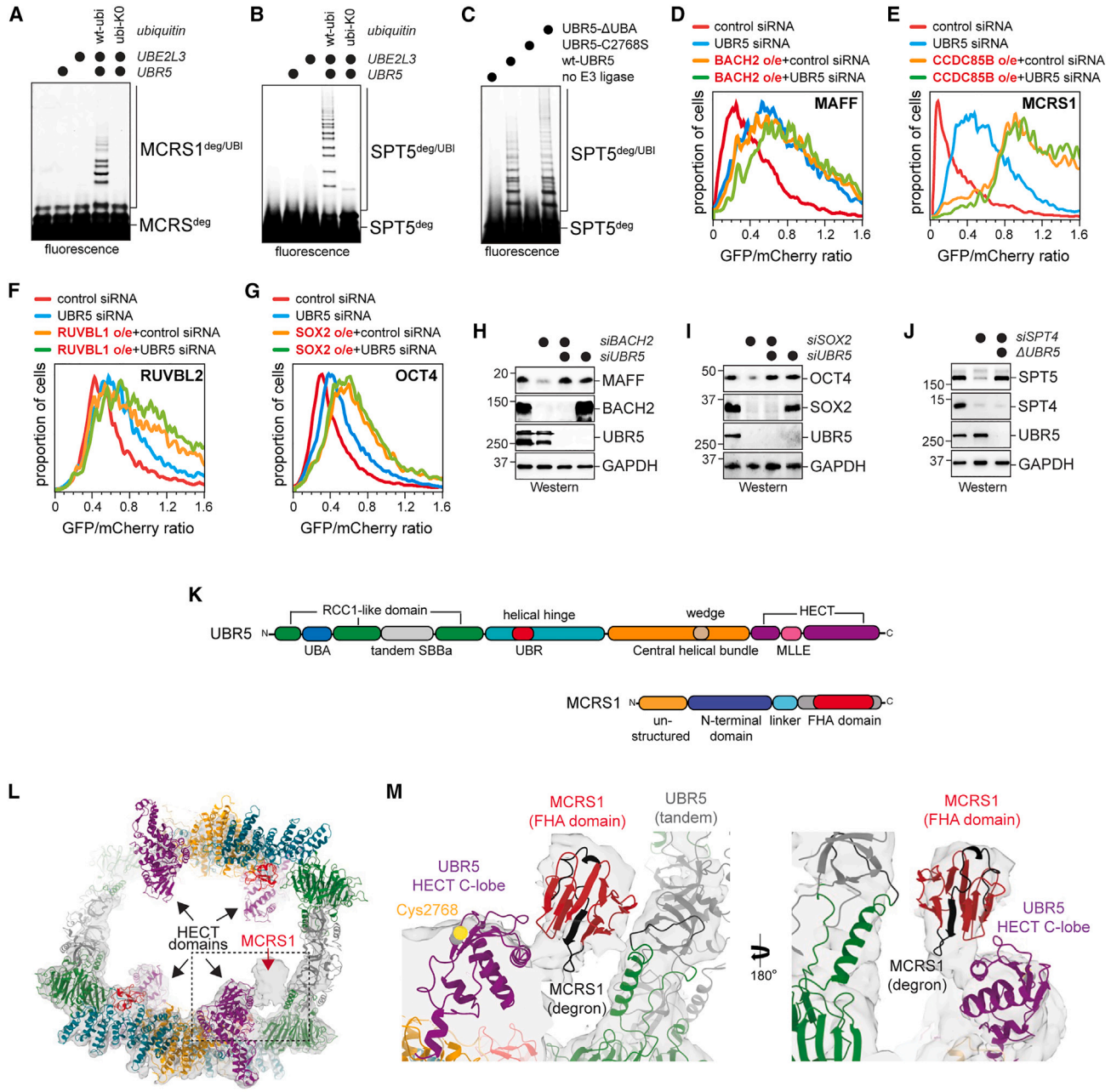

Figure 6. UBR5 provides orphan quality control

(A) UBR5 was incubated with TAMRA-labeled MCRS1 degron, E1, UBE2L3, and ubiquitin. Ubiquitylation was monitored by fluorescence.

(B) UBR5 ubiquitylated TAMRA-labeled SPT5 degron peptides.

(C) UBR5, UBR5^{C2768S}, and UBR5$^{\Delta UBA}$ were incubated with the SPT5 degron, E1, UBE2L3, and ubiquitin.

(D) BACH2 protects MAFF from UBR5-dependent degradation. The MAFF reporter was expressed in cells depleted of UBR5 and/or co-expressing BACH2, as indicated. MAFF stability was determined by flow cytometry.

(E) The MCRS1 reporter is stabilized by CCDC85B.

(F) The RUVBL2 reporter is stabilized by RUVBL1.

(G) The OCT4 reporter is stabilized by SOX2.

(H) BACH2 protects endogenous MAFF from UBR5-dependent degradation. 293T cells were depleted of BACH2 and/or UBR5, and endogenous MAFF was visualized by western blot analysis.

(I) SOX2 protects endogenous OCT4 from UBR5-dependent degradation in H1 hESCs.

(legend continued on next page)

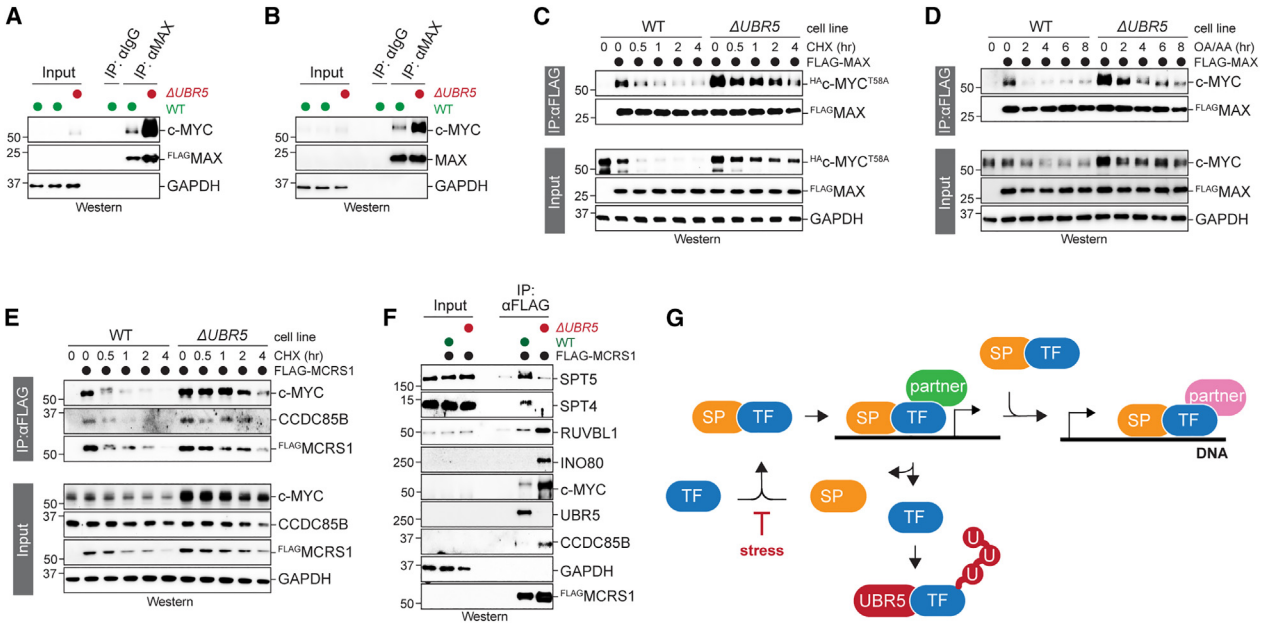

Figure 7. Transcription factor degradation establishes network dynamics

(A) ^{FLAG}MAX was affinity purified using FLAG antibodies from wild-type or *ΔUBR5* HeLa cells, and co-purifying c-Myc was detected by western blot analysis.

(B) Endogenous MAX was precipitated from wild-type or *ΔUBR5* HeLa cells, and co-purifying c-Myc was detected by western blot analysis.

(C) Wild-type or *ΔUBR5* 293T cells expressing ^{FLAG}MAX and ^{HA}c-Myc^{T58A} were treated with cycloheximide. ^{FLAG}MAX was immunoprecipitated, and co-purifying proteins were detected by western blot analysis.

(D) ^{FLAG}MAX was immunoprecipitated from wild-type or *ΔUBR5* cells treated with oligomycin and antimycin A, and co-purifying proteins were detected by western blot analysis.

(E) ^{FLAG}MCRS1 was precipitated from wild-type or *ΔUBR5* 293T cells exposed to cycloheximide, and co-purifying proteins were detected by western blot analysis.

(F) ^{FLAG}MCRS1 was immunoprecipitated from wild-type or *ΔUBR5* cells, and co-purifying proteins were detected by western blot analysis.

(G) Orphan quality control establishes network dynamics required for gene expression. Transcription factors (TFs) in the c-Myc network are continuously produced, form complexes with stabilizing partners (SPs), and drive gene expression. Following dissociation, UBR5 degrades one subunit to render complex disassembly irreversible. The stabilizing partner can be re-used, whereas the unstable subunit must be re-synthesized. This network architecture allows transcription factors to efficiently switch from early to late partners while remaining susceptible to stress-induced inhibition of gene expression.

See also Figure S8.

for preserving hESC identity. Intriguingly, UBR5 supports, rather than restricts, the activity of these transcriptional regulators.

The central player in the UBR5-dependent network is c-Myc, whose stabilization or overexpression causes cancer.[74] Cells, therefore, restrict the activity of c-Myc, and they typically rely on E3 ligases that target its amino-terminal transactivation domain required for gene expression.[66,74–79] The most prominent of these enzymes is SCF^{FBXW7}, and the mutation of *FBXW7* or its cognate c-Myc degron is frequently observed in cancer.[66,75]

Our experiments show that UBR5 is of comparable importance to SCF^{FBXW7} for c-Myc degradation yet differs significantly in its mechanism. Rather than targeting active transcription factors, UBR5 eliminates orphan c-Myc molecules that do not engage DNA. UBR5 establishes its specificity by recognizing degrons that only become available upon the dissociation of c-Myc/MAX dimers. The genetic deletion of *MAX* or chemical inhibition of complex formation also decreases c-Myc levels,[80–82] and we expect that UBR5 degrades c-Myc under these conditions. For proteins that are unstable when released from a partner, such as c-Myc, compounds that cause complex dissociation or improve recognition by orphan E3 ligases could be effective strategies to elicit targeted protein degradation.

In addition to c-Myc, UBR5 targets unpaired subunits of many other stem cell transcription factors. Several of these substrates were required for the expression of UBR5-dependent genes and, when depleted, caused similar phenotypes to those cataloged in DepMap. Moreover, these transcription factors cooperate with c-Myc,[16,32,39,40,44,46,47,67,83] suggesting that they act within a functional network required for accurate gene expression.

(J) Wild-type or *ΔUBR5* 293T cells were depleted of SPT4, and the levels of SPT5 were determined by western blot analysis.

(K) Overview of the domain structures of UBR5 and MCRS1.

(L) Cryo-EM structure of UBR5 bound to MCRS1 at an overall resolution of 4.4 Å.

(M) Detailed view of the interface between UBR5 and the MCRS1 FHA domain.

See also Figures S6 and S7.

UBR5 detects these targets through the same site as c-Myc, and we accordingly found degrons of similar composition in MCRS1 and SPT5. As shown by the structure of MCRS1-bound UBR5, the E3 ligase sandwiches its target between the HECT domain of one subunit and the tandem domain of another subunit of tetrameric UBR5. This architecture is incompatible with substrates being incorporated into larger complexes and thus explains why UBR5 favors the recognition of unpaired proteins.

Suggesting that this regulatory mechanism extends even further, a parallel study noted that UBR5 targets nuclear hormone receptors.[64] These transcription factors engage UBR5 and co-activators through overlapping binding sites, suggesting that in this case also, UBR5 integrates assembly cues into a degradation response. As a tetrameric enzyme, UBR5 could target other proteins in the transcription hubs organized by hormone receptors and establish a similarly dynamic network to the one we had observed for c-Myc.

Orphan quality control promotes gene expression

Revealing an unexpected role for quality control, we found that UBR5 has a regulatory function in shaping interactions at the heart of gene expression. Following the dissociation of transcription factor complexes, UBR5 degrades unpaired subunits and thereby renders complex disassembly irreversible. Cells react to the continuous degradation of orphan subunits with increased resynthesis, thereby creating cycles of complex formation and subunit degradation that establish a dynamic interaction network that can integrate environmental cues into transcriptional programs (Figure 7G).

This mode of regulation offers multiple advantages: it should allow stable subunits, such as MAX, to be recycled to drive gene expression at new promoters or regulate transcription with new partners.[84] c-Myc, SPT5, and MCRS1 also successively engage distinct co-factors, such as chromatin modifiers, RNA polymerases, and elongation factors,[16,51] and cycles of complex formation and orphan subunit degradation facilitate the switch between partners despite the high concentrations in transcription hubs.[24,26] Finally, orphan degradation introduces a need for constant transcription factor synthesis and, thereby, ensures that this machinery remains responsive to changes in cell state, as required for proteins that control cell fate. The role of UBR5 in establishing network dynamics could thus explain why protein degradation is required for transcription.[85–88] In fact, the better a transcription factor stimulates gene expression, the faster it is degraded.[89–92] We propose that orphan degradation optimizes the dynamics of transcriptional networks that must integrate environmental or developmental inputs into coherent outputs. By identifying additional orphan E3 ligases, we, therefore, stand to find new opportunities to modulate gene expression programs and provide therapeutic relief in diseases caused by transcription factor dysregulation.

Limitations of the study

Although our work reveals a regulatory role for orphan quality control in gene expression, the extent to which this pathway controls transcription factors beyond c-Myc still needs to be assessed. Preliminary data suggest that OCT4 is recognized through a motif in its DNA-binding region, but the interplay among OCT4, its partner SOX2, and UBR5 requires further investigation. While our findings imply that small molecules that increase the interaction between UBR5 and orphan transcription factors will downregulate pathological gene expression, developing such molecules to clinically relevant efficacy will require dedicated screening and medicinal chemistry efforts.

STAR★METHODS

Detailed methods are provided in the online version of this paper and include the following:

- KEY RESOURCES TABLE
- RESOURCE AVAILABILITY
  - Lead contact
  - Materials availability
  - Data and code availability
- EXPERIMENTAL MODEL AND STUDY PARTICIPANT DETAILS
- METHOD DETAILS
  - Flow cytometry
  - Immunofluorescence and confocal microscopy
  - Cell synchronization
  - Purification of UBR5
  - In vitro transcription/translation (IVT/T) of substrates
  - UBR5-MCRS1 *in vitro* binding assays
  - In vitro ubiquitylation
  - Mass spectrometry
  - Immunoprecipitation
  - Purification of p97, Ufd and Npl4
  - Pulldown of ubiquitylated substrate by p97-Ufd1-Npl4 complexes
  - Real-time qPCR (qRT-PCR) analysis
  - Generation of CRISPR/Cas9 genome-edited cell lines
  - Guide RNAs for CRISPR/Cas9-mediated genome editing
  - DepMap analysis
  - RNAseq sample preparation and analysis
  - Cryo electron microscopy
  - Integrative model building
  - Crosslinking Mass spectrometry (XL-MS)
- QUANTIFICATION AND STATISTICAL ANALYSIS

SUPPLEMENTAL INFORMATION

Supplemental information can be found online at https://doi.org/10.1016/j.cell.2023.06.015.

ACKNOWLEDGMENTS

We thank all lab members for their ideas, help, and enthusiasm. We are grateful to the UCB Cancer Research Laboratory Flow Cytometry Facility and the Vincent J. Proteomics/Mass Spectrometry Laboratory (NIH S10RR025622). We thank Jan Seebacher from the FMI Protein Analysis Facility for the analysis of cross-linking mass spectrometry. K.G.M. and D.A. were supported by NIH F32 postdoctoral fellowships, S.K. was supported by an NSF predoctoral fellowship, and D.L.H. was supported by a Helen Hay Whitney postdoctoral fellowship. Work in N.H.T.'s lab was funded by Swiss National Science Foundation grants 179541 and 201206 and European Research Council grant 884331. M.R. is an HHMI investigator.

AUTHOR CONTRIBUTIONS

K.G.M., S.K., D.M.G., B.M.-G., and C.X. performed most experiments. D.A. and D.L.H. engineered cell lines. D.L.H. analyzed RNA-seq data. S.K.S. generated p97. J.D.A., S.S., L.K., and G.K. performed structural analyses. K.G.M., S.K., D.M.G., D.L.H., B.M.-G., C.X., N.H.T., and M.R. analyzed the data. K.G.M., S.K., J.D.A., D.M.G., S.S., N.H.T., and M.R. wrote the manuscript.

DECLARATION OF INTERESTS

M.R. is a co-founder and an SAB member of Nurix, Zenith, and Lyterian Therapeutics; an SAB member for Monte Rosa and Vicinitas Therapeutics; and an iPartner at The Column Group. N.H.T. receives funding from the Novartis Research Foundation and is an SAB member of Monte Rosa Therapeutics.

INCLUSION AND DIVERSITY

We support inclusive, diverse, and equitable conduct of research. One or more of the authors of this paper self-identifies as an underrepresented ethnic minority in science.

Received: November 6, 2022
Revised: April 13, 2023
Accepted: June 21, 2023
Published: July 20, 2023; Corrected online: July 28, 2023

REFERENCES

1. Padovani, C., Jevtić, P., and Rapé, M. (2022). Quality control of protein complex composition. Mol. Cell *82*, 1439–1450. https://doi.org/10.1016/j.molcel.2022.02.029.
2. Huttlin, E.L., Bruckner, R.J., Navarrete-Perea, J., Cannon, J.R., Baltier, K., Gebreab, F., Gygi, M.P., Thornock, A., Zarraga, G., Tam, S., et al. (2021). Dual proteome-scale networks reveal cell-specific remodeling of the human interactome. Cell *184*, 3022–3040.e28. https://doi.org/10.1016/j.cell.2021.04.011.
3. Li, J., Cai, Z., Vaites, L.P., Shen, N., Mitchell, D.C., Huttlin, E.L., Paulo, J.A., Harry, B.L., and Gygi, S.P. (2021). Proteome-wide mapping of short-lived proteins in human cells. Mol. Cell *81*, 4722–4735.e5. https://doi.org/10.1016/j.molcel.2021.09.015.
4. Pierce, N.W., Kleiger, G., Shan, S.-o., and Deshaies, R.J. (2009). Detection of sequential polyubiquitylation on a millisecond timescale. Nature *462*, 615–619. https://doi.org/10.1038/nature08595.
5. Toyama, B.H., Savas, J.N., Park, S.K., Harris, M.S., Ingolia, N.T., Yates, J.R., III, and Hetzer, M.W. (2013). Identification of long-lived proteins reveals exceptional stability of essential cellular structures. Cell *154*, 971–982. https://doi.org/10.1016/j.cell.2013.07.037.
6. Liu, X., Reitsma, J.M., Mamrosh, J.L., Zhang, Y., Straube, R., and Deshaies, R.J. (2018). Cand1-mediated adaptive exchange mechanism enables variation in F-box protein expression. Mol. Cell *69*, 773–786.e6. https://doi.org/10.1016/j.molcel.2018.01.038.
7. Harper, J.W., and Schulman, B.A. (2021). Cullin-RING ubiquitin ligase regulatory circuits: a quarter century beyond the F-box hypothesis. Annu. Rev. Biochem. *90*, 403–429. https://doi.org/10.1146/annurev-biochem-090120-013613.
8. Greber, B.J., and Nogales, E. (2019). The structures of eukaryotic transcription pre-initiation complexes and their functional implications. Subcell. Biochem. *93*, 143–192. https://doi.org/10.1007/978-3-030-28151-9_5.
9. Hong, S., Choi, S., Kim, R., and Koh, J. (2020). Mechanisms of macromolecular interactions mediated by protein intrinsic disorder. Mol. Cells *43*, 899–908. https://doi.org/10.14348/molcells.2020.0186.
10. Snead, W.T., and Gladfelter, A.S. (2019). The control centers of biomolecular phase separation: how membrane surfaces, PTMs, and active processes regulate condensation. Mol. Cell *76*, 295–305. https://doi.org/10.1016/j.molcel.2019.09.016.
11. Magits, W., and Sablina, A.A. (2022). The regulation of the protein interaction network by monoubiquitination. Curr. Opin. Struct. Biol. *73*, 102333. https://doi.org/10.1016/j.sbi.2022.102333.
12. Ali, I., Ruiz, D.G., Ni, Z., Johnson, J.R., Zhang, H., Li, P.-C., Khalid, M.M., Conrad, R.J., Guo, X., Min, J., et al. (2019). Crosstalk between RNA Pol II C-terminal domain acetylation and phosphorylation via RPRD proteins. Mol. Cell *74*, 1164–1174.e4. https://doi.org/10.1016/j.molcel.2019.04.008.
13. Manford, A.G., Mena, E.L., Shih, K.Y., Gee, C.L., McMinimy, R., Martínez-González, B., Sherriff, R., Lew, B., Zoltek, M., Rodríguez-Pérez, F., et al. (2021). Structural basis and regulation of the reductive stress response. Cell *184*, 5375–5390.e16.
14. Tan, X., Calderon-Villalobos, L.I.A., Sharon, M., Zheng, C., Robinson, C.V., Estelle, M., and Zheng, N. (2007). Mechanism of auxin perception by the TIR1 ubiquitin ligase. Nature *446*, 640–645. https://doi.org/10.1038/nature05731.
15. Busch, S.J., and Sassone-Corsi, P. (1990). Dimers, leucine zippers and DNA-binding domains. Trends Genet. *6*, 36–40. https://doi.org/10.1016/0168-9525(90)90071-d.
16. Lourenco, C., Resetca, D., Redel, C., Lin, P., MacDonald, A.S., Ciaccio, R., Kenney, T.M.G., Wei, Y., Andrews, D.W., Sunnerhagen, M., et al. (2021). MYC protein interactors in gene transcription and cancer. Nat. Rev. Cancer *21*, 579–591. https://doi.org/10.1038/s41568-021-00367-9.
17. Chen, J., Zhang, Z., Li, L., Chen, B.-C., Revyakin, A., Hajj, B., Legant, W., Dahan, M., Lionnet, T., Betzig, E., et al. (2014). Single-molecule dynamics of enhanceosome assembly in embryonic stem cells. Cell *156*, 1274–1285. https://doi.org/10.1016/j.cell.2014.01.062.
18. Mena, E.L., Jevtić, P., Greber, B.J., Gee, C.L., Lew, B.G., Akopian, D., Nogales, E., Kuriyan, J., and Rape, M. (2020). Structural basis for dimerization quality control. Nature *586*, 452–456. https://doi.org/10.1038/s41586-020-2636-7.
19. Bertolini, M., Fenzl, K., Kats, I., Wruck, F., Tippmann, F., Schmitt, J., Auburger, J.J., Tans, S., Bukau, B., and Kramer, G. (2021). Interactions between nascent proteins translated by adjacent ribosomes drive homomer assembly. Science *371*, 57–64. https://doi.org/10.1126/science.abc7151.
20. Mena, E.L., Kjolby, R.A.S., Saxton, R.A., Werner, A., Lew, B.G., Boyle, J.M., Harland, R., and Rape, M. (2018). Dimerization quality control ensures neuronal development and survival. Science *362*, eaap8236. https://doi.org/10.1126/science.aap8236.
21. Boija, A., Klein, I.A., Sabari, B.R., Dall'Agnese, A., Coffey, E.L., Zamudio, A.V., Li, C.H., Shrinivas, K., Manteiga, J.C., Hannett, N.M., et al. (2018). Transcription factors activate genes through the phase-separation capacity of their activation domains. Cell *175*, 1842–1855.e16. https://doi.org/10.1016/j.cell.2018.10.042.
22. Lu, H., Yu, D., Hansen, A.S., Ganguly, S., Liu, R., Heckert, A., Darzacq, X., and Zhou, Q. (2018). Phase-separation mechanism for C-terminal hyperphosphorylation of RNA polymerase II. Nature *558*, 318–323. https://doi.org/10.1038/s41586-018-0174-3.
23. Trojanowski, J., Frank, L., Rademacher, A., Mücke, N., Grigaitis, P., and Rippe, K. (2022). Transcription activation is enhanced by multivalent interactions independent of phase separation. Mol. Cell *82*, 1878–1893.e10. https://doi.org/10.1016/j.molcel.2022.04.017.
24. Rippe, K., and Papantonis, A. (2022). Functional organization of RNA polymerase II in nuclear subcompartments. Curr. Opin. Cell Biol. *74*, 88–96. https://doi.org/10.1016/j.ceb.2022.01.005.
25. Papantonis, A., and Cook, P.R. (2013). Transcription factories: genome organization and gene regulation. Chem. Rev. *113*, 8683–8705. https://doi.org/10.1021/cr300513p.
26. Wei, M.-T., Chang, Y.-C., Shimobayashi, S.F., Shin, Y., Strom, A.R., and Brangwynne, C.P. (2020). Nucleated transcriptional condensates amplify gene expression. Nat. Cell Biol. *22*, 1187–1196. https://doi.org/10.1038/s41556-020-00578-6.

27. Jackson, D.A., Hassan, A.B., Errington, R.J., and Cook, P.R. (1993). Visualization of focal sites of transcription within human nuclei. EMBO J. *12*, 1059–1065. https://doi.org/10.1002/j.1460-2075.1993.tb05747.x.

28. Chong, S., Graham, T.G.W., Dugast-Darzacq, C., Dailey, G.M., Darzacq, X., and Tjian, R. (2022). Tuning levels of low-complexity domain interactions to modulate endogenous oncogenic transcription. Mol. Cell *82*, 2084–2097.e5. https://doi.org/10.1016/j.molcel.2022.04.007.

29. Osborne, C.S., Chakalova, L., Mitchell, J.A., Horton, A., Wood, A.L., Bolland, D.J., Corcoran, A.E., and Fraser, P. (2007). Myc dynamically and preferentially relocates to a transcription factory occupied by Igh. PLoS Biol. *5*, e192. https://doi.org/10.1371/journal.pbio.0050192.

30. Patel, A., Lee, H.O., Jawerth, L., Maharana, S., Jahnel, M., Hein, M.Y., Stoynov, S., Mahamid, J., Saha, S., Franzmann, T.M., et al. (2015). A liquid-to-solid phase transition of the ALS protein FUS accelerated by disease mutation. Cell *162*, 1066–1077. https://doi.org/10.1016/j.cell.2015.07.047.

31. Wagh, K., Garcia, D.A., and Upadhyaya, A. (2021). Phase separation in transcription factor dynamics and chromatin organization. Curr. Opin. Struct. Biol. *71*, 148–155. https://doi.org/10.1016/j.sbi.2021.06.009.

32. Oh, E., Mark, K.G., Mocciaro, A., Watson, E.R., Prabu, J.R., Cha, D.D., Kampmann, M., Gamarra, N., Zhou, C.Y., and Rape, M. (2020). Gene expression and cell identity controlled by anaphase-promoting complex. Nature *579*, 136–140. https://doi.org/10.1038/s41586-020-2034-1.

33. Meissner, B., Kridel, R., Lim, R.S., Rogic, S., Tse, K., Scott, D.W., Moore, R., Mungall, A.J., Marra, M.A., Connors, J.M., et al. (2013). The E3 ubiquitin ligase UBR5 is recurrently mutated in mantle cell lymphoma. Blood *121*, 3161–3164. https://doi.org/10.1182/blood-2013-01-478834.

34. Qiao, X., Liu, Y., Prada, M.L., Mohan, A.K., Gupta, A., Jaiswal, A., Sharma, M., Merisaari, J., Haikala, H.M., Talvinen, K., et al. (2020). *UBR5* is coamplified with *MYC* in breast tumors and encodes an ubiquitin ligase that limits MYC-dependent apoptosis. Cancer Res. *80*, 1414–1427. https://doi.org/10.1158/0008-5472.CAN-19-1647.

35. Liao, L., Song, M., Li, X., Tang, L., Zhang, T., Zhang, L., Pan, Y., Chouchane, L., and Ma, X. (2017). E3 ubiquitin ligase UBR5 drives the growth and metastasis of triple-negative breast cancer. Cancer Res. *77*, 2090–2101. https://doi.org/10.1158/0008-5472.CAN-16-2409.

36. Song, M., Yeku, O.O., Rafiq, S., Purdon, T., Dong, X., Zhu, L., Zhang, T., Wang, H., Yu, Z., Mai, J., et al. (2020). Tumor derived UBR5 promotes ovarian cancer growth and metastasis through inducing immunosuppressive macrophages. Nat. Commun. *11*, 6298. https://doi.org/10.1038/s41467-020-20140-0.

37. Huttlin, E.L., Bruckner, R.J., Paulo, J.A., Cannon, J.R., Ting, L., Baltier, K., Colby, G., Gebreab, F., Gygi, M.P., Parzen, H., et al. (2017). Architecture of the human interactome defines protein communities and disease networks. Nature *545*, 505–509. https://doi.org/10.1038/nature22366.

38. Jungblut, A., Hopfner, K.-P., and Eustermann, S. (2020). Megadalton chromatin remodelers: common principles for versatile functions. Curr. Opin. Struct. Biol. *64*, 134–144. https://doi.org/10.1016/j.sbi.2020.06.024.

39. Wang, L., Du, Y., Ward, J.M., Shimbo, T., Lackford, B., Zheng, X., Miao, Y.-l., Zhou, B., Han, L., Fargo, D.C., et al. (2014). INO80 facilitates pluripotency gene activation in embryonic stem cell self-renewal, reprogramming, and blastocyst development. Cell Stem Cell *14*, 575–591. https://doi.org/10.1016/j.stem.2014.02.013.

40. Zhou, B., Wang, L., Zhang, S., Bennett, B.D., He, F., Zhang, Y., Xiong, C., Han, L., Diao, L., Li, P., et al. (2016). INO80 governs superenhancer-mediated oncogenic transcription and tumor growth in melanoma. Genes Dev. *30*, 1440–1453. https://doi.org/10.1101/gad.277178.115.

41. Aoi, Y., Takahashi, Y.-H., Shah, A.P., Iwanaszko, M., Rendleman, E.J., Khan, N.H., Cho, B.-K., Goo, Y.A., Ganesan, S., Kelleher, N.L., and Shilatifard, A. (2021). SPT5 stabilization of promoter-proximal RNA polymerase II. Mol. Cell *81*, 4413–4424.e5. https://doi.org/10.1016/j.molcel.2021.08.006.

42. Tastemel, M., Gogate, A.A., Malladi, V.S., Nguyen, K., Mitchell, C., Banaszynski, L.A., and Bai, X. (2017). Transcription pausing regulates mouse embryonic stem cell differentiation. Stem Cell Res. *25*, 250–255. https://doi.org/10.1016/j.scr.2017.11.012.

43. Hu, S., Peng, L., Xu, C., Wang, Z., Song, A., and Chen, F.X. (2021). SPT5 stabilizes RNA polymerase II, orchestrates transcription cycles, and maintains the enhancer landscape. Mol. Cell *81*, 4425–4439.e6. https://doi.org/10.1016/j.molcel.2021.08.029.

44. Baluapuri, A., Hofstetter, J., Dudvarski Stankovic, N., Endres, T., Bhandare, P., Vos, S.M., Adhikari, B., Schwarz, J.D., Narain, A., Vogt, M., et al. (2019). MYC recruits SPT5 to RNA polymerase II to promote processive transcription elongation. Mol. Cell *74*, 674–687.e11. https://doi.org/10.1016/j.molcel.2019.02.031.

45. Ali, A., Veeranki, S.N., Chinchole, A., and Tyagi, S. (2017). MLL/WDR5 complex regulates Kif2A localization to ensure chromosome congression and proper spindle assembly during mitosis. Dev. Cell *41*, 605–622.e7. https://doi.org/10.1016/j.devcel.2017.05.023.

46. Thomas, L.R., Wang, Q., Grieb, B.C., Phan, J., Foshage, A.M., Sun, Q., Olejniczak, E.T., Clark, T., Dey, S., Lorey, S., et al. (2015). Interaction with WDR5 promotes target gene recognition and tumorigenesis by MYC. Mol. Cell *58*, 440–452. https://doi.org/10.1016/j.molcel.2015.02.028.

47. Jiménez Martín, O., Schlosser, A., Furtwängler, R., Wegert, J., and Gessler, M. (2021). MYCN and MAX alterations in Wilms tumor and identification of novel N-MYC interaction partners as biomarker candidates. Cancer Cell Int. *21*, 555. https://doi.org/10.1186/s12935-021-02259-2.

48. Littler, S., Sloss, O., Geary, B., Pierce, A., Whetton, A.D., and Taylor, S.S. (2019). Oncogenic MYC amplifies mitotic perturbations. Open Biol. *9*, 190136. https://doi.org/10.1098/rsob.190136.

49. Schukur, L., Zimmermann, T., Niewoehner, O., Kerr, G., Gleim, S., Bauer-Probst, B., Knapp, B., Galli, G.G., Liang, X., Mendiola, A., et al. (2020). Identification of the HECT E3 ligase UBR5 as a regulator of MYC degradation using a CRISPR/Cas9 screen. Sci. Rep. *10*, 20044. https://doi.org/10.1038/s41598-020-76960-z.

50. Apostolou, E., and Stadtfeld, M. (2018). Cellular trajectories and molecular mechanisms of iPSC reprogramming. Curr. Opin. Genet. Dev. *52*, 77–85. https://doi.org/10.1016/j.gde.2018.06.002.

51. Baluapuri, A., Wolf, E., and Eilers, M. (2020). Target gene-independent functions of MYC oncoproteins. Nat. Rev. Mol. Cell Biol. *21*, 255–267. https://doi.org/10.1038/s41580-020-0215-2.

52. Yau, R.G., Doerner, K., Castellanos, E.R., Haakonsen, D.L., Werner, A., Wang, N., Yang, X.W., Martinez-Martin, N., Matsumoto, M.L., Dixit, V.M., and Rape, M. (2017). Assembly and function of heterotypic ubiquitin chains in cell-cycle and protein quality control. Cell *171*, 918–933.e20. https://doi.org/10.1016/j.cell.2017.09.040.

53. Ohtake, F., Tsuchiya, H., Saeki, Y., and Tanaka, K. (2018). K63 ubiquitylation triggers proteasomal degradation by seeding branched ubiquitin chains. Proc. Natl. Acad. Sci. USA *115*, E1401–E1408. https://doi.org/10.1073/pnas.1716673115.

54. Kolla, S., Ye, M., Mark, K.G., and Rapé, M. (2022). Assembly and function of branched ubiquitin chains. Trends Biochem. Sci. *47*, 759–771. https://doi.org/10.1016/j.tibs.2022.04.003.

55. Manford, A.G., Rodríguez-Pérez, F., Shih, K.Y., Shi, Z., Berdan, C.A., Choe, M., Titov, D.V., Nomura, D.K., and Rape, M. (2020). A cellular mechanism to detect and alleviate reductive stress. Cell *183*, 46–61.e21. https://doi.org/10.1016/j.cell.2020.08.034.

56. Sievers, Q.L., Petzold, G., Bunker, R.D., Renneville, A., Słabicki, M., Liddicoat, B.J., Abdulrahman, W., Mikkelsen, T., Ebert, B.L., and Thomä, N.H. (2018). Defining the human C2H2 zinc finger degrome targeted by thalidomide analogs through CRBN. Science *362*, eaat0572. https://doi.org/10.1126/science.aat0572.

57. Koren, I., Timms, R.T., Kula, T., Xu, Q., Li, M.Z., and Elledge, S.J. (2018). The eukaryotic proteome is shaped by E3 ubiquitin ligases targeting

C-terminal degrons. Cell *173*, 1622–1635.e14. https://doi.org/10.1016/j.cell.2018.04.028.

58. Jares, P., Colomer, D., and Campo, E. (2007). Genetic and molecular pathogenesis of mantle cell lymphoma: perspectives for new targeted therapeutics. Nat. Rev. Cancer *7*, 750–762. https://doi.org/10.1038/nrc2230.
59. Nair, S.K., and Burley, S.K. (2003). X-ray structures of Myc-Max and Mad-Max recognizing DNA. Molecular bases of regulation by proto-oncogenic transcription factors. Cell *112*, 193–205. https://doi.org/10.1016/s0092-8674(02)01284-9.
60. Durocher, D., Henckel, J., Fersht, A.R., and Jackson, S.P. (1999). The FHA domain is a modular phosphopeptide recognition motif. Mol. Cell *4*, 387–394. https://doi.org/10.1016/s1097-2765(00)80340-8.
61. Bernecky, C., Plitzko, J.M., and Cramer, P. (2017). Structure of a transcribing RNA polymerase II-DSIF complex reveals a multidentate DNA-RNA clamp. Nat. Struct. Mol. Biol. *24*, 809–815. https://doi.org/10.1038/nsmb.3465.
62. Hodáková, Z., Grishkovskaya, I., Brunner, H.L., Bolhuis, D.L., Belačić, K., Schleiffer, A., Kotisch, H., Brown, N.G., and Haselbach, D. (2023). Cryo-EM structure of the chain-elongating E3 ligase UBR5. EMBO J, e113348. https://doi.org/10.15252/embj.2022113348.
63. Wang, F., He, Q., Zhan, W., Yu, Z., Finkin-Groner, E., Ma, X., Lin, G., and Li, H. (2023). Structure of the human UBR5 E3 ubiquitin ligase. Structure *31*, 541–552. https://doi.org/10.1016/j.str.2023.03.010.
64. Tsai, J.M., Aguirre, J.D., Li, Y.D., Brown, J., Focht, V., Kater, L., Kempf, G., Sandoval, B., Schmitt, S., Rutter, J., et al. (2023). UBR5 forms ligand-dependent complexes on chromatin to regulate nuclear hormone receptor stability. Mol Cell *83*. https://doi.org/10.1016/j.molcel.2023.06.028.
65. Juszkiewicz, S., and Hegde, R.S. (2018). Quality control of orphaned proteins. Mol. Cell *71*, 443–457. https://doi.org/10.1016/j.molcel.2018.07.001.
66. Welcker, M., Orian, A., Jin, J., Grim, J.E., Harper, J.W., Eisenman, R.N., and Clurman, B.E. (2004). The Fbw7 tumor suppressor regulates glycogen synthase kinase 3 phosphorylation-dependent c-Myc protein degradation. Proc. Natl. Acad. Sci. USA *101*, 9085–9090. https://doi.org/10.1073/pnas.0402770101.
67. Endres, T., Solvie, D., Heidelberger, J.B., Andrioletti, V., Baluapuri, A., Ade, C.P., Muhar, M., Eilers, U., Vos, S.M., Cramer, P., et al. (2021). Ubiquitylation of MYC couples transcription elongation with double-strand break repair at active promoters. Mol. Cell *81*, 830–844.e13. https://doi.org/10.1016/j.molcel.2020.12.035.
68. Jaenicke, L.A., von Eyss, B., Carstensen, A., Wolf, E., Xu, W., Greifenberg, A.K., Geyer, M., Eilers, M., and Popov, N. (2016). Ubiquitin-dependent turnover of MYC antagonizes MYC/PAF1C complex accumulation to drive transcriptional elongation. Mol. Cell *61*, 54–67. https://doi.org/10.1016/j.molcel.2015.11.007.
69. Harper, J.W., and Bennett, E.J. (2016). Proteome complexity and the forces that drive proteome imbalance. Nature *537*, 328–338. https://doi.org/10.1038/nature19947.
70. Hipp, M.S., Park, S.-H., and Hartl, F.U. (2014). Proteostasis impairment in protein-misfolding and -aggregation diseases. Trends Cell Biol. *24*, 506–514. https://doi.org/10.1016/j.tcb.2014.05.003.
71. Brehme, M., Voisine, C., Rolland, T., Wachi, S., Soper, J.H., Zhu, Y., Orton, K., Villella, A., Garza, D., Vidal, M., et al. (2014). A chaperome subnetwork safeguards proteostasis in aging and neurodegenerative disease. Cell Rep. *9*, 1135–1150. https://doi.org/10.1016/j.celrep.2014.09.042.
72. Kaushik, S., and Cuervo, A.M. (2015). Proteostasis and aging. Nat. Med. *21*, 1406–1415. https://doi.org/10.1038/nm.4001.
73. Vilchez, D., Simic, M.S., and Dillin, A. (2014). Proteostasis and aging of stem cells. Trends Cell Biol. *24*, 161–170. https://doi.org/10.1016/j.tcb.2013.09.002.
74. Welcker, M., and Clurman, B.E. (2008). FBW7 ubiquitin ligase: a tumour suppressor at the crossroads of cell division, growth and differentiation. Nat. Rev. Cancer *8*, 83–93. https://doi.org/10.1038/nrc2290.
75. Reavie, L., Della Gatta, G., Crusio, K., Aranda-Orgilles, B., Buckley, S.M., Thompson, B., Lee, E., Gao, J., Bredemeyer, A.L., Helmink, B.A., et al. (2010). Regulation of hematopoietic stem cell differentiation by a single ubiquitin ligase-substrate complex. Nat. Immunol. *11*, 207–215. https://doi.org/10.1038/ni.1839.
76. Welcker, M., Wang, B., Rusnac, D.-V., Hussaini, Y., Swanger, J., Zheng, N., and Clurman, B.E. (2022). Two diphosphorylated degrons control c-Myc degradation by the Fbw7 tumor suppressor. Sci. Adv. *8*, eabl7872. https://doi.org/10.1126/sciadv.abl7872.
77. Adhikary, S., Marinoni, F., Hock, A., Hulleman, E., Popov, N., Beier, R., Bernard, S., Quarto, M., Capra, M., Goettig, S., et al. (2005). The ubiquitin ligase HectH9 regulates transcriptional activation by Myc and is essential for tumor cell proliferation. Cell *123*, 409–421. https://doi.org/10.1016/j.cell.2005.08.016.
78. King, B., Boccalatte, F., Moran-Crusio, K., Wolf, E., Wang, J., Kayembe, C., Lazaris, C., Yu, X., Aranda-Orgilles, B., Lasorella, A., and Aifantis, I. (2016). The ubiquitin ligase Huwe1 regulates the maintenance and lymphoid commitment of hematopoietic stem cells. Nat. Immunol. *17*, 1312–1321. https://doi.org/10.1038/ni.3559.
79. Huber, A.-L., Papp, S.J., Chan, A.B., Henriksson, E., Jordan, S.D., Kriebs, A., Nguyen, M., Wallace, M., Li, Z., Metallo, C.M., and Lamia, K.A. (2016). CRY2 and FBXL3 cooperatively degrade c-MYC. Mol. Cell *64*, 774–789. https://doi.org/10.1016/j.molcel.2016.10.012.
80. Hishida, T., Nozaki, Y., Nakachi, Y., Mizuno, Y., Okazaki, Y., Ema, M., Takahashi, S., Nishimoto, M., and Okuda, A. (2011). Indefinite self-renewal of ESCs through Myc/Max transcriptional complex-independent mechanisms. Cell Stem Cell *9*, 37–49. https://doi.org/10.1016/j.stem.2011.04.020.
81. Blackwood, E.M., Lüscher, B., and Eisenman, R.N. (1992). Myc and Max associate *in vivo*. Genes Dev. *6*, 71–80. https://doi.org/10.1101/gad.6.1.71.
82. Yao, R., Zhang, M., Zhou, J., Liu, L., Zhang, Y., Gao, J., and Xu, K. (2022). Novel dual-targeting c-Myc inhibitor D347-2761 represses myeloma growth via blocking c-Myc/Max heterodimerization and disturbing its stability. Cell Commun. Signal. *20*, 73. https://doi.org/10.1186/s12964-022-00868-6.
83. Guarnaccia, A.d., and Tansey, W.P. (2018). Moonlighting with WDR5: a cellular multitasker. J. Clin. Med. *7*, 21. https://doi.org/10.3390/jcm7020021.
84. Grandori, C., Cowley, S.M., James, L.P., and Eisenman, R.N. (2000). The Myc/Max/Mad network and the transcriptional control of cell behavior. Annu. Rev. Cell Dev. Biol. *16*, 653–699. https://doi.org/10.1146/annurev.cellbio.16.1.653.
85. Ferdous, A., Gonzalez, F., Sun, L., Kodadek, T., and Johnston, S.A. (2001). The 19S regulatory particle of the proteasome is required for efficient transcription elongation by RNA polymerase II. Mol. Cell *7*, 981–991. https://doi.org/10.1016/s1097-2765(01)00250-7.
86. Kinyamu, H.K., and Archer, T.K. (2007). Proteasome activity modulates chromatin modifications and RNA polymerase II phosphorylation to enhance glucocorticoid receptor-mediated transcription. Mol. Cell. Biol. *27*, 4891–4904. https://doi.org/10.1128/MCB.02162-06.
87. Huang, W., Pi, L., Liang, W., Xu, B., Wang, H., Cai, R., and Huang, H. (2006). The proteolytic function of the Arabidopsis 26S proteasome is required for specifying leaf adaxial identity. Plant Cell *18*, 2479–2492. https://doi.org/10.1105/tpc.106.045013.
88. Heidelberger, J.B., Voigt, A., Borisova, M.E., Petrosino, G., Ruf, S., Wagner, S.A., and Beli, P. (2018). Proteomic profiling of VCP substrates links VCP to K6-linked ubiquitylation and c-Myc function. EMBO Rep. *19*, e44754. https://doi.org/10.15252/embr.201744754.

89. Salghetti, S.E., Muratani, M., Wijnen, H., Futcher, B., and Tansey, W.P. (2000). Functional overlap of sequences that activate transcription and signal ubiquitin-mediated proteolysis. Proc. Natl. Acad. Sci. USA *97*, 3118–3123. https://doi.org/10.1073/pnas.050007597.

90. Salghetti, S.E., Caudy, A.A., Chenoweth, J.G., and Tansey, W.P. (2001). Regulation of transcriptional activation domain function by ubiquitin. Science *293*, 1651–1653. https://doi.org/10.1126/science.1062079.

91. Wang, X., Arceci, A., Bird, K., Mills, C.A., Choudhury, R., Kernan, J.L., Zhou, C., Bae-Jump, V., Bowers, A., and Emanuele, M.J. (2017). VprBP/DCAF1 regulates the degradation and nonproteolytic activation of the cell cycle transcription factor FoxM1. Mol. Cell. Biol. *37*, e00609-16. https://doi.org/10.1128/MCB.00609-16.

92. Wu, R.-C., Feng, Q., Lonard, D.M., and O'Malley, B.W. (2007). SRC-3 coactivator functional lifetime is regulated by a phospho-dependent ubiquitin time clock. Cell *129*, 1125–1140. https://doi.org/10.1016/j.cell.2007.04.039.

93. Deutsch, E.W., Bandeira, N., Perez-Riverol, Y., Sharma, V., Carver, J.J., Mendoza, L., Kundu, D.J., Wang, S., Bandla, C., Kamatchinathan, S., et al. (2023). The ProteomeXchange consortium at 10 years: 2023 update. Nucleic Acids Res. *51*, D1539–D1548. https://doi.org/10.1093/nar/gkac1040.

94. Perez-Riverol, Y., Bai, J., Bandla, C., García-Seisdedos, D., Hewapathirana, S., Kamatchinathan, S., Kundu, D.J., Prakash, A., Frericks-Zipper, A., Eisenacher, M., et al. (2022). The PRIDE database resources in 2022: a hub for mass spectrometry-based proteomics evidences. Nucleic Acids Res. *50*, D543–D552. https://doi.org/10.1093/nar/gkab1038.

95. Schindelin, J., Arganda-Carreras, I., Frise, E., Kaynig, V., Longair, M., Pietzsch, T., Preibisch, S., Rueden, C., Saalfeld, S., Schmid, B., et al. (2012). Fiji: an open-source platform for biological-image analysis. Nat. Methods *9*, 676–682. https://doi.org/10.1038/nmeth.2019.

96. Meyer, H.J., and Rape, M. (2014). Enhanced protein degradation by branched ubiquitin chains. Cell *157*, 910–921.

97. Stark, H. (2010). GraFix: stabilization of fragile macromolecular complexes for single particle cryo-EM. Methods Enzymol. *481*, 109–126. https://doi.org/10.1016/S0076-6879(10)81005-5.

98. Schenk, A.D., Cavadini, S., Thomä, N.H., and Genoud, C. (2020). Live analysis and reconstruction of single-particle cryo-electron microscopy data with CryoFLARE. J. Chem. Inf. Model. *60*, 2561–2569. https://doi.org/10.1021/acs.jcim.9b01102.

99. Punjani, A., Rubinstein, J.L., Fleet, D.J., and Brubaker, M.A. (2017). cryoSPARC: algorithms for rapid unsupervised cryo-EM structure determination. Nat. Methods *14*, 290–296. https://doi.org/10.1038/nmeth.4169.

100. Scheres, S.H. (2012). RELION: implementation of a Bayesian approach to cryo-EM structure determination. J. Struct. Biol. *180*, 519–530. https://doi.org/10.1016/j.jsb.2012.09.006.

101. Jakobi, A.J., Wilmanns, M., and Sachse, C. (2017). Model-based local density sharpening of cryo-EM maps. Elife *6*, e27131. https://doi.org/10.7554/eLife.27131.

102. Varadi, M., Anyango, S., Deshpande, M., Nair, S., Natassia, C., Yordanova, G., Yuan, D., Stroe, O., Wood, G., Laydon, A., et al. (2022). AlphaFold Protein Structure Database: massively expanding the structural coverage of protein-sequence space with high-accuracy models. Nucleic Acids Res. *50*, D439–D444. https://doi.org/10.1093/nar/gkab1061.

103. Pettersen, E.F., Goddard, T.D., Huang, C.C., Meng, E.C., Couch, G.S., Croll, T.I., Morris, J.H., and Ferrin, T.E. (2021). UCSF ChimeraX: structure visualization for researchers, educators, and developers. Protein Sci. *30*, 70–82. https://doi.org/10.1002/pro.3943.

104. Marze, N.A., Roy Burman, S.S., Sheffler, W., and Gray, J.J. (2018). Efficient flexible backbone protein-protein docking for challenging targets. Bioinformatics *34*, 3461–3469. https://doi.org/10.1093/bioinformatics/bty355.

105. Croll, T.I. (2018). ISOLDE: a physically realistic environment for model building into low-resolution electron-density maps. Acta Crystallogr. D Struct. Biol. *74*, 519–530. https://doi.org/10.1107/S2059798318002425.

106. Afonine, P.V., Poon, B.K., Read, R.J., Sobolev, O.V., Terwilliger, T.C., Urzhumtsev, A., and Adams, P.D. (2018). Real-space refinement in PHENIX for cryo-EM and crystallography. Acta Crystallogr. D Struct. Biol. *74*, 531–544. https://doi.org/10.1107/S2059798318006551.

107. Combe, C.W., Fischer, L., and Rappsilber, J. (2015). xiNET: cross-link network maps with residue resolution. Mol. Cell. Proteomics *14*, 1137–1147. https://doi.org/10.1074/mcp.O114.042259.

STAR★METHODS

KEY RESOURCES TABLE

REAGENT or RESOURCE	SOURCE	IDENTIFIER
Antibodies		
Rabbit polyclonal anti-ATF3 (D2Y5W)	Cell Signaling Technology	Cat#33593S
Rabbit monoclonal anti-BACH2 (D3T3G)	Cell Signaling Technology	Cat#80775S; RRID: AB_2799961
Rabbit polyclonal anti-BUB1	Bethyl Laboratories	Cat#A300-373A; RRID: AB_2065943
Rabbit polyclonal anti-BUB3	Cell Signaling Technology	Cat#3049S; RRID: AB_2228142
Rabbit polyclonal anti-BUBR1	Bethyl Laboratories	Cat#A300-386A; RRID: AB_386097
Rabbit polyclonal anti-c-Myc	Cell Signaling Technology	Cat#9402S; RRID: AB_2151827
Rabbit polyclonal anti-CCDC85B	Proteintech	Cat#18282-1-AP; RRID: AB_2878527
Rabbit monoclonal anti-CDC20 (D6C2Q)	Cell Signaling Technology	Cat#14866S; RRID: AB_2715567
Rabbit monoclonal anti-Flag DYKDDDDK Tag (D6W5B)	Cell Signaling Technology	Cat#14793S; RRID: AB_2572291
Mouse monoclonal ANTI-FLAG M2®	Sigma-Aldrich	Cat#F1804; RRID: AB_262044
Rabbit monoclonal anti-GAPDH (14C10)	Cell Signaling Technology	Cat#2118S; RRID: AB_561053
Rabbit monoclonal anti-Geminin (E5Q9S) XP®	Cell Signaling Technology	Cat#52508S
Rabbit monoclonal anti-HA tag (C29F4)	Cell Signaling Technology	Cat#3724S; RRID: AB_1549585
Rabbit polyclonal anti-INO80	Bethyl Laboratories	Cat#A303-370A; RRID: AB_10953492
Rabbit polyclonal anti-INO80C	Abcam	Cat#ab151046
Rabbit polyclonal anti-KIF2A	Bethyl Laboratories	Cat#A300-914A; RRID: AB_2280872
Rabbit polyclonal anti-MAFF	ABclonal	Cat#A12920; RRID: AB_2759766
Mouse monoclonal anti-MAX (H-2)	Santa Cruz Biotechnology	Cat#SC-8011; RRID: AB_627913
Rabbit polyclonal anti-MAX (S20)	Cell Signaling Technology	Cat#4739S; RRID: AB_2281777
Rabbit polyclonal anti-MCRS1	Proteintech	Cat#11362-1-AP; RRID: AB_2143116
Rabbit polyclonal anti-NPL4	Cell Signaling Technology	Cat#13489S; RRID: AB_2798232
Rabbit polyclonal anti-NFIL3	Abcam	Cat#ab93785; RRID: AB_10563337
Rabbit polyclonal anti-NPL4	Cell Signaling Technology	Cat#13489S; RRID: AB_2798232
Rabbit polyclonal anti-Pontin/RUVBL1	Cell Signaling Technology	Cat#12300S; RRID: AB_2797876
Rabbit polyclonal anti-SOX2	STEMCELL Technologies	Cat#60055
Rabbit monoclonal anti-SPT4 (D3P2W)	Cell Signaling Technology	Cat#64828S; RRID: AB_2756442
Rabbit polyclonal anti-SUPT5H	Bethyl Laboratories	Cat#A300-869A; RRID: AB_609484
Rabbit polyclonal anti-TAF1A	Thermo Fisher Scientific	Cat#PA5-101172; RRID: AB_2850615
Mouse monoclonal anti-EDD1 (UBR5)	Santa Cruz Biotechnology	Cat#sc-515494
Rabbit polyclonal anti-EDD1 (UBR5)	Bethyl Laboratories	Cat#A300-573A; RRID: AB_2210189

(*Continued on next page*)

Continued

REAGENT or RESOURCE	SOURCE	IDENTIFIER
Rabbit polyclonal anti-UFD1	Cell Signaling Technology	Cat#13789S; RRID: AB_2798313
Rabbit polyclonal anti-Vinculin	Cell Signaling Technology	Cat#4650S; RRID: AB_10559207
Rabbit monoclonal anti-WDR5 (D9E1I)	Cell Signaling Technology	Cat#13105S; RRID: AB_2620133
Goat anti-Mouse IgG (H+L), Superclonal™ Recombinant Secondary Antibody, Alexa Fluor™ 488	Thermo Fisher Scientific	Cat#A28175; RRID:AB_2536161
Hoechst 33342	Anaspec	Cat#AS-83218
Bacterial and virus strains		
One Shot™ Stbl3™ Chemically Competent *E. coli*	Thermo Fisher Scientific	Cat#C737303
Chemicals, peptides, and recombinant proteins		
TAMRA-labeled MYC-degron1 peptide (TEENVKRRTHNVLERQRRNELKRSFFA LRDQIPEK-(5,6-TAMRA))	Thermo Fisher Scientific	N/A
TAMRA-labeled MYC-BR wild type peptide (5,6-TAMRA- TEENVKRRTHNVLERQRRNEL KRSFFALRDQIPEK)	Thermo Fisher Scientific	N/A
TAMRA-labeled MYC-HLHLZ wild type peptide (5,6-TAMRA-KAPKVVILKKATAYILSVQAEEQKLI SEEDLLRKRREQLKHKLEQLRNSCA)	Thermo Fisher Scientific	N/A
TAMRA-labeled MCRS1-degron peptide (5,6-TAMRA-DVDLSLEGPAWKISRKQGVIKLKNNGD)	Thermo Fisher Scientific	N/A
TAMRA-labeled SPT5-degron peptide (5,6-TAMRA -RIKARMSLKDWFAKRKKFKRPPQRLFDAEK)	Thermo Fisher Scientific	N/A
Recombinant Human E1/UBA1 Protein	Laboratory of Michael Rapé	N/A
Recombinant Human UbcH7/UBE2L3 Protein, CF	R&D Systems	Cat#E2-640-100
Recombinant Human Ubiquitin Protein, CF	R&D Systems	Cat#U-100H
Recombinant Human Ubiquitin Mutant No K Protein, CF	R&D Systems	Cat#UM-NOK
Recombinant Human Ubiquitin Mutant K6R Protein, CF	R&D Systems	Cat#UM-K6R
Recombinant Human Ubiquitin Mutant K11R Protein, CF	R&D Systems	Cat#UM-K11R
Recombinant Human Ubiquitin Mutant K27R Protein, CF	R&D Systems	Cat#UM-K27R
Recombinant Human Ubiquitin Mutant K29R Protein, CF	R&D Systems	Cat#UM-K29R
Recombinant Human Ubiquitin Mutant K33R Protein, CF	R&D Systems	Cat#UM-K33K
Recombinant Human Ubiquitin Mutant K48R Protein, CF	R&D Systems	Cat# UM-K48R
Recombinant Human Ubiquitin Mutant with K48 only Protein, CF	R&D Systems	Cat#-UM-K480
Recombinant Human Ubiquitin Mutant K63R Protein, CF	R&D Systems	Cat#-UMK63R
Creatine phosphate	Sigma-Aldrich	Cat#10621714001-5G
L-[35S]-Methionine, 1mCi (37MBq), Specific Activity:>800Ci (29.6TBq)/mMole, 50mM Tricine, 10mM BME	PerkinElmer	Cat#NEG009H001MC
Polyethylenimine (PEI), Linear, MW 25000, Transfection Grade	Polysciences	Cat#23966-1

(*Continued on next page*)

Continued

REAGENT or RESOURCE	SOURCE	IDENTIFIER
cOmplete™, EDTA-free protease inhibitor cocktail tablets from Roche	Sigma-Aldrich	Cat#11873580001
Roche PhosSTOP™	Sigma-Aldrich	Cat#4906845001
3X FLAG® Peptide	Sigma-Aldrich	Cat#F4799
Carfilzomib (PR-171)	Selleck Chemicals	Cat#S2853
Oligomycin A	Santa Cruz Biotechnology	Cat#sc-201551A
Cycloheximide	Sigma-Aldrich	Cat#C7698-5G
Antimycin A, Antibiotic	Abcam	Cat#ab141904
Actinomycin D	Sigma-Aldrich	Cat#A9415
PYR-41	Selleck Chemicals	Cat#S7129
Bafilomycin A1 (Baf-A1)	Selleck Chemicals	Cat#S1413
MG132	Selleck Chemicals	Cat#S2619
NMS-873	Selleck Chemicals	Cat#S7285
Dimethyl Sulfoxide	Fisher Scientific	Cat#BP231-100
Critical commercial assays		
Pierce 660nm Protein Assay Reagent	Thermo Fisher	Cat#22660
Ionic Detergent Compatibility Reagent for Pierce 660nm Protein Assay Reagent	Thermo Fisher	Cat#22663
TnT® Quick Coupled Transcription/ Translation System (SP6 promoter)	Promega	Cat#L2080
Dual-Luciferase® Reporter Assay System	Promega	Cat#E1910
Deposited data		
RNAseq of HEK 293T cells depleted of UBR5	GEO: GSE234200	N/A
Cryo-EM density map	EMD-17541	N/A
Crosslink mass spectrometry	PXD041519	N/A
Experimental models: Cell lines		
HEK293T	UCB Tissue Culture Facility	RRID:SCR_017924
HEK293T-ΔUBR5	This paper	N/A
HeLa	ATCC	RRID:CVCL_0030
HeLa-ΔUBR5	This paper	N/A
HeLa-Flag-UBR5	This paper	N/A
HeLa-Flag-UBR5	This paper	N/A
HeLa-Flag-UBR5ΔHECT-HA	This paper	N/A
HeLa-Flag-UBR5ΔUBA	This paper	N/A
WA01 (H1)	WiCell	RRID:CVCL_9771
Oligonucleotides		
Primer: sgUBR5 exon2 Forward: caccgttacaaaagatctgtacacg	This paper	N/A
Primer: sgUBR5 exon2 Reverse: aaaccgtgtacagatcttttgtaac	This paper	N/A
Primer: sgUBR5 exon3 Forward: caccgtactaattagtttcacactc	This paper	N/A
Primer: sgUBR5 exon3 Reverse: aaacgagtgtgaaactaattagtac	This paper	N/A
Primer: sgUBR5 for 3xFlag knock-in Forward: caccgcacgaaatggatggacgtca	This paper	N/A
Primer: sgUBR5 for 3xFlag knock-in Reverse: aaactgacgtccatccatttcgtgc	This paper	N/A
Primer: sgUBR5 for ΔHECT-HA knock-in Forward: Caccgaagatgttggagcagaacc	This paper	N/A

(*Continued on next page*)

Continued

REAGENT or RESOURCE	SOURCE	IDENTIFIER
Primer: sgUBR5 for ΔHECT-HA knock-in Reverse: aaacggttctgctccaacatcttc	This paper	N/A
Primer: sgUBR5 for ΔUBA knock-in 5' Forward: caccgaataactcgagtctgccggc	This paper	N/A
Primer: sgUBR5 for ΔUBA knock-in 5' Reverse: aaacgccggcagactcgagttattc	This paper	N/A
Primer: sgUBR5 for ΔUBA knock-in 3' Forward: caccgtgatgaagatggagatgatg	This paper	N/A
Primer: sgUBR5 for ΔUBA knock-in 3' Reverse: aaaccatcatctccatcttcatcac	This paper	N/A
Donor oligo DNA for 3xFLAG tag insertion at the N- terminus of UBR5: gggctgggggcgg gcgagagcgggaggggccgccctcgagtggaggacga gaaggaaagcaccatgGACTACAAGGACCACGAC GGTGACTACAAGGACCACGACATCGACTACA AGGACGACGACGACAAGacgtccatccatttcgtgg ttcacccgctgccgggcaccgaggaccagctcaatgac aggtaatag	This paper	N/A
Donor oligo DNA for deletion of the HECT domain (2210-2799) of UBR5 and addition of a C-terminal 3xHA tag: ttctttagaactgttcggcag ggtattcatggaagatgttggagcagaacctggatcaTACC CATACGATGTTCCAGATTACGCTTATCCTTAT GACGTACCTGACTATGCATACCCTTATGAT GTACCAGACTACGCTtaggtatgtattttgtgcacctt aaattccattctgcctgataagcatgtatttcagggaa	This paper	N/A
Donor oligo DNA for deletion of the UBA domain (180-230) of UBR5: gtcatcagctggagctcgagattcccgccggcagact cgagttattcggacaggacgggatcgagggtctgggc ttttgggcagtcagccccagccagttggagatgatggg gatgatacagccagcgaatcttatttgcctggaggttgg tggatcaccgtcatgtttttctcatttctggagtgctctttcgactggg	This paper	N/A
Recombinant DNA		
pCS2-MCRS1-GFP-IRES-mCherry	This paper	N/A
pCS2-Myc-GFP-IRES-mCherry	This paper	N/A
pCS2-Myc(Δ1-429)-GFP-IRES-mCherry (ΔTAD)	This paper	N/A
pCS2-Myc(Δ1-429; Δ340-439)-GFP-IRES-mCherry (ΔTADΔDBD)	This paper	N/A
pCS2-NLS-Myc(340-439)-GFP-IRES-mCherry (NLS-DBD)	This paper	N/A
pCS2-NES-Myc(340-439)-GFP-IRES-mCherry (NES-DBD)	This paper	N/A
pCS2-Myc(Δ1-429; K355E; R356E; R357E; Y402A; I403A; L404A; S405A; V406A; L434E; C438E)-GFP-IRES-mCherry (ΔTADΔDeg1ΔDeg2)	This paper	N/A
pCS2-Myc(Δ1-429; K355E; R356E; R357E)-GFP-IRES-mCherry (ΔTADΔDeg1)	This paper	N/A
pCS2-Myc(Δ1-429; K355E; R356E; R357E; Δ398-439)-GFP-IRES-mCherry (ΔTADΔDeg1ΔLZ)	This paper	N/A
pCS2-CDC20-GFP-IRES-mCherry	This paper	N/A
pCS2-POU5F2-GFP-IRES-mCherry	This paper	N/A
pCS2-INO80C-GFP-IRES-mCherry	This paper	N/A
pCS2-NFIL3-GFP-IRES-mCherry	This paper	N/A

(*Continued on next page*)

Continued

REAGENT or RESOURCE	SOURCE	IDENTIFIER
pCS2-RUVBL2-GFP-IRES-mCherry	This paper	N/A
pCS2-TAF1A-GFP-IRES-mCherry	This paper	N/A
pCS2-ATF3-GFP-IRES-mCherry	This paper	N/A
pCS2-INO80B-GFP-IRES-mCherry	This paper	N/A
pCS2-NRL-GFP-IRES-mCherry	This paper	N/A
pCS2-SPT5-GFP-IRES-mCherry	This paper	N/A
pCS2-SPT4-GFP-IRES-mCherry	This paper	N/A
pCS2-AKIRIN2-GFP-IRES-mCherry	This paper	N/A
pCS2-GEMININ-GFP-IRES-mCherry	This paper	N/A
pCS2-SMARCB1-GFP-IRES-mCherry	This paper	N/A
pCS2-OCT4-GFP-IRES-mCherry	This paper	N/A
pCS2-DDIT3-GFP-IRES-mCherry	This paper	N/A
pCS2-HIF1α-GFP-IRES-mCherry	This paper	N/A
pCS2-SECURIN-GFP-IRES-mCherry	This paper	N/A
pCS2-CCNB1-GFP-IRES-mCherry	This paper	N/A
pCS2-CDC73-GFP-IRES-mCherry	This paper	N/A
pCS2-NEK2A-GFP-IRES-mCherry	This paper	N/A
pCS2-ATF5-GFP-IRES-mCherry	This paper	N/A
pCS2-FOXA3-GFP-IRES-mCherry	This paper	N/A
pCS2-CEBPG-GFP-IRES-mCherry	This paper	N/A
pCS2-ESRRG-GFP-IRES-mCherry	This paper	N/A
pCS2-CREB3L2-GFP-IRES-mCherry	This paper	N/A
pCS2-CREBZF-GFP-IRES-mCherry	This paper	N/A
pCS2-POU2F2-GFP-IRES-mCherry	This paper	N/A
pCS2-AURKA-GFP-IRES-mCherry	This paper	N/A
pCS2-KATNA1-GFP-IRES-mCherry	This paper	N/A
pCS2-BMAL1B-GFP-IRES-mCherry	This paper	N/A
pCS2-CIB1-GFP-IRES-mCherry	This paper	N/A
pCS2-KLF4-GFP-IRES-mCherry	This paper	N/A
pCS2-GATA3-GFP-IRES-mCherry	This paper	N/A
pCS2-SPI1-GFP-IRES-mCherry	This paper	N/A
pCS2-NRF2-GFP-IRES-mCherry	This paper	N/A
pCS2-TRF1-GFP-IRES-mCherry	This paper	N/A
pCS2-FOSL2-GFP-IRES-mCherry	This paper	N/A
pCS2-HDAC3-GFP-IRES-mCherry	This paper	N/A
pCS2-YY1-GFP-IRES-mCherry	This paper	N/A
pCS2-JUNB-GFP-IRES-mCherry	This paper	N/A
pCS2-PAIP2-GFP-IRES-mCherry	This paper	N/A
pCS2-TCF-GFP-IRES-mCherry	This paper	N/A
pCS2-RNF168-GFP-IRES-mCherry	This paper	N/A
pCS2-HLF-GFP-IRES-mCherry	This paper	N/A
pCS2-FBXO28-GFP-IRES-mCherry	This paper	N/A
pCS2-MycN-GFP-IRES-mCherry	This paper	N/A
pCS2-MycL-GFP-IRES-mCherry	This paper	N/A
pCS2-INO80E-GFP-IRES-mCherry	This paper	N/A
pCS2-MAFB-GFP-IRES-mCherry	This paper	N/A
pCS2-TFIIS-GFP-IRES-mCherry	This paper	N/A
pCS2-TFAP2A-GFP-IRES-mCherry	This paper	N/A
pCS2-CEBPE-GFP-IRES-mCherry	This paper	N/A

(*Continued on next page*)

Continued

REAGENT or RESOURCE	SOURCE	IDENTIFIER
pCS2-CEBPB-GFP-IRES-mCherry	This paper	N/A
pCS2-ATF4-GFP-IRES-mCherry	This paper	N/A
pCS2-RUVBL1-GFP-IRES-mCherry	This paper	N/A
pCS2-ZNF789-GFP-IRES-mCherry	This paper	N/A
pCS2-TRPC4AP-GFP-IRES-mCherry	This paper	N/A
pCS2-USF1-GFP-IRES-mCherry	This paper	N/A
pCS2-CLOCK-GFP-IRES-mCherry	This paper	N/A
pCS2-MYF5-GFP-IRES-mCherry	This paper	N/A
pCS2-MAFG-GFP-IRES-mCherry	This paper	N/A
pCS2-NFE2L1-GFP-IRES-mCherry	This paper	N/A
pCS2-SOX2-GFP-IRES-mCherry	This paper	N/A
pCS2-ARF-GFP-IRES-mCherry	This paper	N/A
pCS2-POU3F4-GFP-IRES-mCherry	This paper	N/A
pCS2-ACTR5-GFP-IRES-mCherry	This paper	N/A
pCS2-PAF1-GFP-IRES-mCherry	This paper	N/A
pCS2-ZNF354B-GFP-IRES-mCherry	This paper	N/A
pCS2-TRA13-GFP-IRES-mCherry	This paper	N/A
pCS2-ZNF616-GFP-IRES-mCherry	This paper	N/A
pCS2-TRIM28-GFP-IRES-mCherry	This paper	N/A
pCS2-ACTR3B-GFP-IRES-mCherry	This paper	N/A
pCS2-MAX-GFP-IRES-mCherry	This paper	N/A
pCS2-MAD2-GFP-IRES-mCherry	This paper	N/A
pCS2-BUB3-GFP-IRES-mCherry	This paper	N/A
pCS2-PRB1-GFP-IRES-mCherry	This paper	N/A
pCS2-BUBR1-GFP-IRES-mCherry	This paper	N/A
pCS2-FOSL1-GFP-IRES-mCherry	This paper	N/A
pCS2-CREB5-GFP-IRES-mCherry	This paper	N/A
pCS2-BACH2-GFP-IRES-mCherry	This paper	N/A
pCS2-MXD1-GFP-IRES-mCherry	This paper	N/A
pCS2-TLE3-GFP-IRES-mCherry	This paper	N/A
pCS2-RPAP3-GFP-IRES-mCherry	This paper	N/A
pCS2-CREB3-GFP-IRES-mCherry	This paper	N/A
pCS2-EPAS1-GFP-IRES-mCherry	This paper	N/A
pCS2-JUND-GFP-IRES-mCherry	This paper	N/A
pCS2-ZNF30-GFP-IRES-mCherry	This paper	N/A
pCS2-NANOG-GFP-IRES-mCherry	This paper	N/A
pCS2-ZNF506-GFP-IRES-mCherry	This paper	N/A
pCS2-CIB1-GFP-IRES-mCherry	This paper	N/A
pCS2-UCHL5-GFP-IRES-mCherry	This paper	N/A
pCS2-CREB1-GFP-IRES-mCherry	This paper	N/A
pCS2-ATF2-GFP-IRES-mCherry	This paper	N/A
pCS2-MAFK-GFP-IRES-mCherry	This paper	N/A
pCS2-FOXA1-GFP-IRES-mCherry	This paper	N/A
pCS2-JUN-GFP-IRES-mCherry	This paper	N/A
pCS2-GTF21-GFP-IRES-mCherry	This paper	N/A
pCS2-CREB3L4-GFP-IRES-mCherry	This paper	N/A
pCS2-NFE2L2-GFP-IRES-mCherry	This paper	N/A
pCS2-ATF7-GFP-IRES-mCherry	This paper	N/A
pCS2-MYOD1-GFP-IRES-mCherry	This paper	N/A

(*Continued on next page*)

Continued

REAGENT or RESOURCE	SOURCE	IDENTIFIER
pCS2-FOS-GFP-IRES-mCherry	This paper	N/A
pCS2-PIRH2-GFP-IRES-mCherry	This paper	N/A
pCS2-CREB3L1-GFP-IRES-mCherry	This paper	N/A
pCS2-ATF1-GFP-IRES-mCherry	This paper	N/A
pCS2-ASCL1-GFP-IRES-mCherry	This paper	N/A
pCS2-BACH1-GFP-IRES-mCherry	This paper	N/A
pCS2-CDK9-GFP-IRES-mCherry	This paper	N/A
pCS2-SP1-GFP-IRES-mCherry	This paper	N/A
pCS2-p27-GFP-IRES-mCherry	This paper	N/A
pCS2-ATF6B-GFP-IRES-mCherry	This paper	N/A
pCS2-2xEsp3I-GFP-IRES-mCherry	This paper	N/A
pCS2-MAX	This paper	N/A
pCS2-Myc	This paper	N/A
pCS2-RUVBL2	This paper	N/A
pCS2-MCRS1	This paper	N/A
pCS2-CCDC85B	This paper	N/A
pCS2-CDC20	This paper	N/A
pCS2-SPT4	This paper	N/A
pCS2-SPT5	This paper	N/A
pCS2-SOX2	This paper	N/A
pCS2-MAD2	This paper	N/A
pCS2-BUB1	This paper	N/A
pCS2-BUBR1	This paper	N/A
pCS2-BUB3	This paper	N/A
pCS2-BACH2	This paper	N/A
pCS2-ATF3	This paper	N/A
pCS2-INO80C	This paper	N/A
pCS2-NFIL3	This paper	N/A
pCS2-SMARCB1	This paper	N/A
pCS2-NRL	This paper	N/A
pCS2-JUNB	This paper	N/A
pCS2-CEBPB	This paper	N/A
pCS2-HA-Myc	This paper	N/A
pCS2-HA-Myc(K355E; R356E; R357E; Y402A; I403A; L404A; S405A; V406A; L434E; C438E) (c-Myc-Δdeg)	This paper	N/A
pCS2-HA-SPT5	This paper	N/A
pCMV-FLAG-MAX	This paper	N/A
pCMV-FLAG-MCRS1	This paper	N/A
pCMV-FLAG-MCRS1ΔFHA	This paper	N/A
pCMV-FLAG-MYC	This paper	N/A
pCMV-FLAG-CCDC85B	This paper	N/A
pCMV-FLAG-UBR5	This paper	N/A
pCMV-FLAG-UBR5(C2768S)	This paper	N/A
pCMV-FLAG-UBR5(ΔUBA)	This paper	N/A
pCS2-MCRS1-4XUbΔgg	This paper	N/A
Software and algorithms		
GraphPad Prism 9	GraphPad Software Inc.	RRID:SCR_002798
FlowJo 10.8.1	FlowJo	RRID:SCR_008520

(*Continued on next page*)

Continued

REAGENT or RESOURCE	SOURCE	IDENTIFIER
CompPASS	Huttlin et al.[37]	N/A
Zen Blue	ZEN Digital Imaging for Light Microscopy	RRID:SCR_013672
Fiji ImageJ2 version 2.9.0/1.53t	Fiji	RRID:SCR_002285
Jupyter Notebook version 6.4.12	Jupyter	RRID:SCR_018315
Other		
Lipofectamine™ RNAiMAX	Thermo Fisher Scientific	Cat#13778150
Lipofectamine™ 3000 Transfection reagent	Thermo Fisher Scientific	Cat#L3000008
ANTI-FLAG® M2 Affinity Agarose Gel slurry	Sigma-Aldrich	Cat#A2220
EZview™ Red Anti-HA Affinity Gel	Sigma-Aldrich	Cat#E6779-1ML
Lenti-X™ Concentrator	Takara	Cat#631232
Protein A Agarose	Sigma-Aldrich	Cat#11134515001
Protein G Agarose	Sigma-Aldrich	Cat#11719416001
Pierce™ Silver Stain Kit	Thermo Fisher Scientific	Cat#24612

RESOURCE AVAILABILITY

Lead contact

Further information and requests for reagents and resources should be directed to Michael Rapé (mrape@berkeley.edu).

Materials availability

All plasmids and cell lines generated in this work can be requested from the lead contact's lab and will be freely shared. All antibodies, chemicals, and most cell lines used in this study are commercially available.

Data and code availability

- Original gene expression data obtained by RNA-seq from HEK 293T cells and H1 human embryonic stem cells lacking UBR5 were uploaded to GEO with accession code GEO: GSE234200 and are publicly available. The cryo-EM density map has been deposited at the Electron Microscopy Data Bank database and is publicly available with accession code EMD-17541. The corresponding integrative model was deposited at the Zenodo database under the following https://doi.org/10.5281/zenodo.7997361. The crosslink mass spectrometry data are publicly available and have been deposited to the ProteomeXchange Consortium[93] via the PRIDE partner repository[94] with the dataset identifier PXD041519.
- This paper does not report original code.
- Any additional information required to reanalyze the data reported in this work paper is available from the lead contact upon request.

EXPERIMENTAL MODEL AND STUDY PARTICIPANT DETAILS

Human embryonic kidney (HEK) 293T and HeLa cells were maintained in DMEM + GlutaMAX (Gibco, 10566-016) supplemented with 10% fetal bovine serum (VWR, 89510-186). Plasmid transfections for immunoprecipitations were performed using polyethylenimine (PEI) at a 1:3 ratio of DNA (in μg) to PEI (in μl at a 1 mg ml^{-1} stock concentration). siRNA transfections were performed using 20 nM of indicated siRNAs and 5ul of RNAiMAX transfection reagent (Thermo Fisher, 13778150) per well in a 6-well cell culture plate. Lentiviruses were produced in HEK 293T cells by co-transfection of lentiviral and packaging plasmids using Lipofectamine® 3000 transfection reagent (Thermo, L3000015). Viruses were harvested 48 h post transfection, concentrated using the Lenti-X concentrator (Takara, 631232), aliquoted, and stored at −80°C for later use. HEK 293T cells were purchased directly from the Berkeley Cell Culture Facility (authenticated by short tandem repeat analysis). HeLa cells were not authenticated.

Recombinant UBR5 for biochemical and structural studies were produced in HEK293F cells via transient expression using the Expi293 Expression System Kit (Thermo Fisher, A14635) according to the manufacturer's protocol. Recombinant UBR5 HECT domain constructs were produced in E. coli BL21-CodonPlus(DE3)-RIL cells grown in LB broth media. Recombinant MCRS1 proteins were produced in Trichoplusia ni (High Five) and Spodoptera frugiperda (Sf9) insect cells cultured at 27°C in SF4 Baculo Express Media (BioConcept, 9-00F38-K).

Human embryonic stem cells (WiCell, WA01/H1) were grown in mTeSR™1 media (StemCell Technologies, 85850) on hESC-qualified Matrigel-coated plates (Corning, 354277) with daily media change. H1s were passaged by Accutase (StemCell Technologies, 07920) for siRNA transfections, lentiviral infections, or routine maintenance. For siRNA transfections, single cell suspensions of H1s

were generated by Accutase treatment and 2–5×10^5 cells were seeded on a Matrigel-coated well of a 6-well plate with 1.8 ml of mTeSR™1 containing 10 μM of Y-27632 (StemCell Technologies, 72308) and a 0.2 ml mixture of indicated siRNAs (at a final concentration of 20 nM) and 5ul of RNAiMAX transfection reagent buffered in Opti-MEM per well in a 6-well cell culture plate. For lentiviral infections, single cell suspensions of H1s were generated by Accutase treatment and 1.5–3×10^5 cells were seeded on a Matrigel-coated well of a 6-well plate with 2 ml of mTeSR™1 containing 10 μM of Y-27632, polybrene (at a final concentration of 8 μg/ml), and lentiviruses produced from HEK 293T cells (see above) for 2 h. The media was immediately exchanged with 2 ml of fresh mTeSR™1 containing 10 μM of Y-27632 only. hESCs were drug-selected 24–48 h post infection.

All cell lines were routinely tested for mycoplasma contamination using the Mycoplasma PCR Detection Kit (abmGood, G238).

METHOD DETAILS

Flow cytometry

HeLa cells were seeded at 300,000 cells per well in 6-well plates. siRNAs were reverse transfected (at the time of seeding cells) with 20 nM of indicated siRNAs and 5ul of RNAiMAX transfection reagent (Thermo Fisher, 13778150) per well in a 6-well cell culture plate. The next day, 0.33 μg of ^{GFP}degron-IRES-mCherry reporters, 2 μg of overexpression constructs, and empty vector up to maximum of 5 μg (without co-transfection, the total was 2 μg per well) total were combined and transfected into each well using Lipofectamine 3000 (ThermoFisher, L3000008) per manufacturer's instructions. After 24 h, cells were harvested for flow cytometry. Cells were treated with the following reagents at indicated times before harvesting: 2 μM Carfilzomib (Selleck, PR-171) for 6 h, 700 nM Bafilomycin A1 for 6 h (Selleck, S1413), 1 μM MLN-4924 (Selleck, S7109) for 6 h, or 10 μM NMS-873 (Selleck, S7285) for 6 h. At 24 h post-transfection, cells were trypsinized and centrifuged at 300×g for 5 min. Cells were resuspended in DMEM with 10% FBS and analyzed on either BD Bioscience LSR Fortessa or LSR Fortessa X20 and FlowJo.

Immunofluorescence and confocal microscopy

Flag-UBR5 HeLa cells were seeded on 12mm glass coverslips at 175,000 cells/well in a 12-well plate. Cells were reverse transfected immediately following seeding with indicated siRNAs 20μM (40nM final concentration). Media was changed on all plates 24h after transfection. 48h after transfection cells were fixed in a solution of 4% paraformaldehyde in 1X dPBS for 30min, followed by permeabilization with 0.1% Triton X-100 in 1X dPBS for 20min, and finally blocked with 3% BSA in 1X dPBS for 1h. Samples were probed with anti-Flag M2 antibody (1:500) for 4h in 1X dPBS containing 0.1% Tween-20 and 1% BSA. Followed primary incubation, samples were incubated with secondary antibody AF488 (1:500) and stained with Hoechst 33342 (1:3000) for 1h. All sample processing was carried out at room temperature. Coverslips were mounted onto microscope slides with ProLong gold antifade reagent and imaged using a Zeiss LSM 900 with Airyscan 2 microscope. Images were captures with a 63x oil objective and Airyscan SR. Images were processed using Zen Blue (Zeiss) airyscan processing and Fiji.[95]

Cell synchronization

CRISPR/Cas9-edited ^{FLAG}UBR5 HeLa cells were synchronized as previously described.[32] Cells were synchronized in S phase by addition of 2 mM thymidine for 24 h, washed with 1×PBS, and harvested by scraping. To arrest cells in prometaphase, S phase-arrested cells were subsequently washed with 1XPBS to remove excess thymidine and released into fresh media (DMEM/10% FBS) for 3 h, then treated with 5 μM S-trityl-L-cysteine (Sigma, 164739) for 12–14 h. Prometaphase cells were collected by vigorous pipetting and washed with 1×PBS. Cell pellets were either immediately used in immunoprecipitation assays or frozen in liquid nitrogen and stored at −80°C for later use.

Purification of UBR5

For *in vitro* ubiquitylations, human UBR5 enzyme was purified from extracts of CRISPR/Cas9-edited ^{FLAG}UBR5 HeLa cells. Harvested prometaphase pellets were lysed in lysis buffer (20 mM HEPES, pH 7.4, 5 mM KCl, 150 mM NaCl, 1.5 mM $MgCl_2$, 0.1% Nonidet P-40, 1X cOmplete™ protease inhibitor cocktail (Roche, 04693159001), 2 μM carfilzomib (Selleck, PR-171) and 1 μl of benzonase (Millipore, 70746) per 15-cm plate). Detergent lysed cells were then subjected to a high-speed spin (20,000×*g*) to remove cellular debris and the clarified extract was pre-cleared with protein A-agarose resin (Roche, 11719408001). UBR5 was purified with anti-FLAG® M2 affinity resin (Sigma, A2220) for 1.5 h at 4°C. UBR5-coupled beads were washed 5× with lysis buffer (minus inhibitors and benzonase) prior to use. To quantify the amount and purity of ^{FLAG}UBR5, a Pierce™ Silver Stain Kit was used per manufacturer's instructions (Thermo Fisher Scientific, 24612).

For cryo EM, full-length human UBR5 was cloned with an N-terminal FLAG tag into a pDEST-CMV vector (Thermo Fisher) and transiently expressed in HEK293F mammalian cells (Thermo Fisher, A14527). Therefore, protein expression was performed in a 0.5 L suspension culture according to the Expi293 expression system (Thermo Fisher, A14635). The cells were harvested three days post-infection and lysed in 60 ml "lysis buffer" (25 mM HEPES pH 7.6, 150 mM KCl, 5 mM $MgCl_2$, 0.5 mM $CaCl_2$, 5% glycerol, 0.1% TRITON X-100). Subsequently, the lysate was cleared by ultracentrifugation at 35 K rpm for 45 minutes, filtered, and incubated with 5 ml of FLAG M2 gel (Sigma-Aldrich, A2220) for 2 hours at 4°C. After sequential washing of the protein-bound beads with "wash buffer" (25 mM HEPES pH 7.6, 5% glycerol, 0.05% TWEEN-20) supplemented with 700 mM KCl and 300 mM KCl, elution was performed with "wash buffer" supplemented with 300 mM KCl and 0.3 mg/ml 3xFLAG peptide (Sigma-Aldrich, F4799). The

UBR5-containing fractions after FLAG elution were directly applied to a Mono Q 5/50 GL column (Cytiva, 17516601) equilibrated in "wash buffer" supplemented with 300 mM KCl and 0.5 mM TCEP. The protein was eluted in a linear gradient from 300 mM to 800 mM KCl, concentrated, and injected onto a Superose 6 column (Cytiva, 29091596) equilibrated in "SEC buffer" (25 mM HEPES pH 7.6, 150 mM KCl, 0.5 mM TCEP, and 5% glycerol).

The UBR5 HECT domain constructs were cloned into bacterial pET28a vectors and expressed as N-terminal His_{10}-SUMO tag proteins in *E. coli* BL21-(DE3)-RIL cells (Agilent, 230245). Full-length and truncated MCRS1 constructs were cloned into a pAC8-derived vector and expressed as STREP-SUMO-tagged proteins in High Five insect cells (Thermo Fisher, B85502). In brief, the cleared supernatant after ultracentrifugation was used for affinity purification either using a HisTrap FF column (Cytiva, 17525501) or StrepTactin (IBA lifesciences, 2-1201-025). In the case of UBR5 HECT constructs, the His_{10}-SUMO tag was removed by TEV cleavage overnight. As a final polishing step, proteins were purified by size exclusion chromatography on a Superdex200 (Cytiva, 28-9893-35) in 50 mM HEPES pH 7.5, 200 mM NaCl, 0.5 mM TCEP, and 5% Glycerol.

In vitro transcription/translation (IVT/T) of substrates

All *in vitro* synthesized substrates were cloned under the SP6 promoter. The corresponding plasmids can be found in the key resources table. ^{35}S-labeled substrates were generated by incubating 583 ng of plasmid DNA in 14 μl of rabbit reticulocyte lysate (Promega, L2080) supplemented with 2 μM carfilzomib and 0.3 μl of ^{35}S-Met (PerkinElmer, NEG009H001MC) for 1 h at 30°C. ^{35}S-labeled substrates were used for *in vitro* ubiquitylation assays.

UBR5-MCRS1 *in vitro* binding assays

Binding assays in the presence of FLAG-UBR5 were performed using 12 μl of FLAG M2 slurry (Sigma-Aldrich, A2220) equilibrated in assay buffer (25 mM HEPES pH 7.4, 150 mM NaCl and 0.05% TWEEN-20). After the resin was pelleted, the excess buffer was removed and replaced with 100 μl of fresh assay buffer, followed by the addition of 15 pmol (2.5 μl of 6 μM protein stock) FLAG-UBR5. After incubation at 4°C for 90 minutes, the supernatant was again removed, and 100 μL of fresh assay buffer was added, together with 150 pmol of the respective STREP-SUMO-MCRS1 construct. The protein-bound resin was incubated for another 90 minutes, followed by three sequential washing steps with 400 μl of assay buffer each. The protein elution took place in 45 μl of assay buffer supplemented with 1 mg/ml 3xFLAG peptide. (Sigma-Aldrich, F4799) on a rotating wheel at room temperature for 60 minutes. Subsequently, 20 ul of the supernatant was mixed with 6 μl 5xSDS gel loading buffer. 10 μl of each sample was applied to a 4-20% SDS-PAGE gradient gel (Bio-Rad, 4561096). After gel electrophoresis, the gel was transferred to a nitrocellulose membrane (Bio-Rad, 1704158) using the Trans-Blot Turbo Transfer System (Bio-Rad). Following blocking with 5% skim milk solution in TBST buffer, the membrane was incubated with an Anti-STREP primary antibody (IBA lifesciences, 2-1507-001) and incubated at 4°C overnight. The next day, the membrane was washed thrice with TBST buffer and incubated with an Alexa Fluor790 conjugated secondary antibody (Invitrogen, A11357), followed by three additional washes with TBST. The final imaging of the membrane was done on a Li-COR Odyssey DLx imaging system (Li-COR, Biosciences) at 800 nm.

For binding assays in the presence of the UBR5 HECT constructs, 7.5 μL MagStrep "type 3" XT beads slurry (IBA lifesciences, 2-4090-002) were equilibrated in assay buffer. Following buffer removal and the addition of 14 μL fresh assay buffer, 60 pmol of STREP-SUMO-MCRS1 full length was added to the resin (6 μL of 10 μM protein stock). After 60 min of incubation on a rotating wheel at 4°C, the supernatant was replaced by 12 μL fresh assay buffer and 200 pmol of the respective HECT construct (8 μL of 25 μM protein stock). After an additional hour of incubation, the supernatant was removed, and the resin was washed three times with 200 μL assay buffer. Proteins were eluted in 25 μL of 1x SDS sample buffer, whereby 20 μL of each elution was applied to SDS-PAGE on a 4-20% gradient gel (Biorad, 4561096) for analysis.

In vitro ubiquitylation

In vitro ubiquitylation assays were performed in a 10 μl reaction volume: 0.5 μl of 10 μM E1 (250 nM final), 1 μl of 25 μM E2 (2.5 μM final), 1 μl of 10 mg ml^{-1} ubiquitin (1 mg ml^{-1} final) (R&D Systems, U-100H), 1 μl of 100 mM DTT, 1.5 μl of energy mix (150 mM creatine phosphate, 20 mM ATP, 20 mM $MgCl_2$, 2 mM EGTA, pH to 7.5 with KOH), 1 μl of 1×PBS, 1 μl of 10× ubiquitylation assay buffer (250 mM Tris 7.5, 500 mM NaCl, and 100 mM $MgCl_2$), and 3 μl of substrate (*in vitro* translated or recombinant) were pre-mixed and added to 10 μl of UBR5-coupled bed resin, equivalent to ~2.5μM UBR5 (see section purification of UBR5). Reactions were performed at 30°C with shaking for 2 h unless noted otherwise. Reactions were stopped by adding 2X urea sample buffer and resolved on SDS-acrylamide gels prior to autoradiography. E1 was purified as described in Meyer and Rape (2014)[96] while commercially available UBE2D3 (R&D Systems, E2-627-100) and UBE2L3 (R&D Systems, E2-640-100) were used. Contrast of gel images has been adjusted, if necessary, across the entire image to detect the specific modified peptide signal.

Mass spectrometry

Mass spectrometry was performed on immunoprecipitates prepared from HEK 293T or HeLa cells. For immunoprecipitations of overexpressed proteins, thirty 15-cm plates of HEK 293T cells were PEI-transfected, grown to confluence, harvested, and lysed in lysis buffer (20 mM HEPES, pH 7.4, 5 mM KCl, 150 mM NaCl, 1.5 mM $MgCl_2$, 0.1% Nonidet P-40, and 1× cOmplete™ protease inhibitor cocktail). For endogenous UBR5 IPs, one hundred 15-cm plates of CRISPR/Cas9-edited ^{FLAG}UBR5 HEK 293T or HeLa cells were used. Lysed extracts were clarified by high-speed centrifugation, pre-cleared with protein A-agarose slurry and bound to

anti-FLAG® M2 affinity resin. IPs were then washed and eluted 3× at 30°C with 0.5 mg ml^{-1} of 3×FLAG® peptide (Sigma, F4799) buffered in 1×PBS plus 0.1% Triton X-100. Elutions were pooled and precipitated overnight at 4°C with 20% trichloroacetic acid. IPs were then pelleted, washed 3× with an ice-cold acetone/0.1 N HCl solution, dried, resolubilized in 8 M urea buffered in 100 mM Tris 8.5, reduced with TCEP (at a final concentration of 5 mM) for 20 min, alkylated with iodoacetamide (at a final concentration of 10 mM) for 15 min, diluted four-fold with 100 mM Tris 8.5, and digested with 0.5 mg ml^{-1} of trypsin supplemented with $CaCl_2$ (at a final concentration of 1 mM) overnight at 37°C. Trypsin-digested samples were submitted to the Vincent J. Coates Proteomics/Mass Spectrometry Laboratory at UC Berkeley for analysis. Peptides were processed using multidimensional protein identification technology (MudPIT) and identified using a LTQ XL linear ion trap mass spectrometer. To identify high confidence interactors, CompPASS analysis of the query mass spectrometry result was performed against mass spectrometry results from unrelated FLAG immunoprecipitates performed in our laboratory. Scatter plots were generated using GraphPad Prism 9.

Immunoprecipitation

Human ^{FLAG}UBR5 complexes were immunoprecipitated from endogenously FLAG-tagged HeLa cell lines grown on 15-cm plates to near-confluency. Alternatively, overexpression constructs of FLAG-tagged bait proteins were PEI-transfected into HEK 293T or wild-type HeLa cells with 10 μg of each plasmid per 15-cm plate for 48 h prior to harvesting. Where applicable, cells were treated with either 10 μM carfilzomib for 6 h, with a combination of 10 μM oligomycin A and 2 μM antimycin A, or with 100 μg/ml cycloheximide for the times indicated before harvesting. Cells were harvested by scraping and pellets were lysed in lysis buffer (20 mM HEPES, pH 7.4, 5 mM KCl, 150 mM NaCl, 1.5 mM $MgCl_2$, 0.1% Nonidet P-40, 1× cOmplete™ protease inhibitor cocktail (Roche, 04693159001), supplemented with 1 μl of benzonase (Millipore, 70746) per 15-cm plate). Detergent lysed cells were then subjected to a high speed spin (20,000 × *g*) to remove cellular debris and the clarified extract was pre-cleared with protein A-agarose resin (Sigma-Aldrich, 11134515001). Bait proteins were purified with anti-FLAG® M2 affinity resin (Sigma, A2220) for 1.5 h at 4°C. For *in vitro* ubiquitylation reactions, ^{FLAG}UBR5-coupled beads were washed 5× with lysis buffer (minus inhibitors and benzonase) prior to use. For western blots, FLAG beads with captured bait protein were eluted at 30°C with 0.5 mg ml^{-1} of 3×FLAG® peptide (Sigma, F4799) buffered in 1×PBS plus 0.1% Triton X-100 for 20 min, shaking. Eluates were combined with 2× urea sample buffer (120 mM Tris pH 6.8, 4% SDS, 4 M urea, 20% glycerol, bromophenol blue) prior to SDS-PAGE. For sequential immunoprecipitations, eluates were resuspended in lysis buffer and incubated with EZview™ Red Anti-HA Affinity Gel (Sigma, E6779-1ML) for 3 hr at 4°C. Captured protein was eluted with 2× urea sample buffer (120 mM Tris pH 6.8, 4% SDS, 4 M urea, 20% glycerol, bromophenol blue) prior to SDS-PAGE.

For immunoprecipitation of endogenous UBR5 from H1 hESCs, bait protein was purified using protein G-agarose resin (Sigma-Aldrich, 11719416001) coupled with mouse anti-UBR5 antibody (Santa Cruz Biotechnology, sc-515494), in lysis buffer for 1 h, rotating at 4°C.

Purification of p97, Ufd and Npl4

Human p97 was subcloned into pET28a His-tagged expression vector (pET28a-6xHis-FLAG-TEV-p97) and were expressed in LOBSTR-BL21(DE3)-RIL competent cells. Human Ufd1 and Npl4 were subcloned into a pET28a His-tagged expression vector (pET28a-Ufd1-6xHis) and a pMAL expression vector (pMAL-Npl4) respectively and co-expressed in LOBSTR- BL21(DE3)-RIL competent cells. Protein expression was induced at log phase with 500 μM IPTG for 16 hours at 18°C. Cells were lysed in Lysis buffer (100mM Tris pH 7.4, 500 mM KCl, 5 mM $MgCl_2$, 20 mM imidazole, 5 mM BME, 5% glycerol, and protease inhibitors) using a LM10 Microfluidizer. Lysate was clarified prior to a 1h incubation with equilibrated Ni-NTA agarose beads (Qiagen, Cat# 20350), and beads were washed in wash buffer (50 mM HEPES pH 7.4, 150mM KCl, 5 mM $MgCl_2$, 5 mM BME, 20mM imidazole and 2.5% glycerol). p97 was eluted in wash buffer containing 250 mM imidazole.

Imidazole-eluted fractions containing p97, Ufd1 or Npl4 were confirmed by Coomassie-stained SDS-PAGE were subject to further separation on a HiLoad 26/600 Superdex 200 size exclusion chromatography column (Cytiva, Cat# 28989336) in SEC buffer (20 mM HEPES, pH 7.4, 150 mM KCl, 1mM $MgCl_2$, and 2.5% glycerol) and peak fractions were collected and concentrated with Centricon® Plus-70 Centrifugal Filter Units (Millipore, Cat# UFC703008), filter sterilized, and snap frozen in PBS at -80°C.

Pulldown of ubiquitylated substrate by p97-Ufd1-Npl4 complexes

In vitro ubiquitylation reactions were performed as described in the relevant section. Three reactions of ubiquitylated substrate were used per pulldown. Purified p97, Ufd1, and Npl4 were diluted to 8 μg ml^{-1} in binding buffer (20 mM HEPES pH 7.4, 150 mM KCl, 1mM $MgCl_2$, 0.05% NP-40) and incubated with ubiquitylated material for 1 h at 4°C. Complexes were combined with 10 μl of anti-FLAG® M2 affinity resin (Sigma, A2220) for 1.5 h at 4°C. Beads were washed five times with binding buffer and resuspended in 2× urea sample buffer (120 mM Tris pH 6.8, 4% SDS, 4 M urea, 20% glycerol, bromophenol blue) prior to SDS-PAGE and autoradiography.

Real-time qPCR (qRT-PCR) analysis

For qRT–PCR analysis, total RNA was purified from cells using the NucleoSpin® RNA kit (Macherey-Nagel, no. 740955). For each sample, 1 μg of total RNA was reverse transcribed using the RevertAid First Strand cDNA Synthesis kit (ThermoFisher, K1622) and then diluted either 10-fold (H1 cells) or 20-fold (293T cells) for qRT-PCR. Expression levels were quantified using the Roche KAPA SYBR FAST qPCR Kit (Roche, KK4602) on a Roche LightCycler® 480 II. Graphs were generated using GraphPad Prism 9. qRT-PCR primers used in this study can be found in Table S2.

Generation of CRISPR/Cas9 genome-edited cell lines

All cell lines used in this publication were generated from HEK 293T cells or HeLa cells. Guide RNA sequences were designed using the online resource provided by the Zhang Lab at MIT (http://crispr.mit.edu). The sequences of the genes for editing were obtained from the UCSC Genome browser. The oligonucleotides for guide RNAs (listed in the key resources table) and their complementary sequences were ordered from IDT, annealed, and cloned into a pX330 vector according to the protocol at https://benchling.com/protocols/5DmqRd/crispr-mediated-gene-disruption-in-ch12f3-2-cells/sbs.

Cells were cultured in a 6-well plate at 50% confluence and were transfected using Mirus TransIT-293 transfection reagent (for 293T editing) or Lipofectamine® 3000 transfection reagent (for HeLa editing) using pX330 plasmids (2 μg of total DNA) encoding a guide RNA for site-specific gene cutting. Three days post-transfection, a sample of transfected cells was treated with DNA extraction solution (QuickExtract, Epicenter) and editing was assessed by PCR amplification of the sequence of interest using specific PCR primers. Clonal selection was performed by seeding the cells into 96-well plates at one cell per well density, allowing the single cells to expand, and editing was checked by PCR/sequencing. Clones were validated using western blotting with specific antibodies.

Guide RNAs for CRISPR/Cas9-mediated genome editing

For knockout of the UBR5 locus, a pair of RNA guides was used to remove part of the second and third exons of the *UBR5* locus in HEK 293T cells and HeLa cells: TTACAAAAGATCTGTACACG (Exon 2) and TACTAATTAGTTTCACACTC (Exon 3). For removal of the HECT or UBA domain from Flag-UBR5 HeLa cells, a single guide RNA was used: AAGATGTTGGAGCAGAACC (ΔHECT) or AATAA CTCGAGTCTGCCGGC (ΔUBA).

DepMap analysis

A list of genes composed of the top 21 UBR5 substrates, along with all genes encoding the human Mediator complex, were assembled in a text file called "substrates.txt". Publicly available gene dependency data ("CRISPR_(DepMap_22Q2_Public+Score,_Chronos)_subsetted.csv", DepMap Public 22Q2 dataset) was downloaded from: https://depmap.org/portal/download/all/. The heatmap was generated using these two files and the Python code provided in Table S3 in the open-source Jupyter Notebook interface.

RNAseq sample preparation and analysis

Wild-type and ΔUBR5 HEK 293T cells were grown in a 6-well plate and collected for transcriptomic analysis. For each sample, two independent biological replicates, each with three technical replicates, were harvested. Total RNA was extracted from cells using the NucleoSpin® RNA kit (Macherey-Nagel, no. 740955) according to the manufacturer's instructions. Library preparation and sequencing was performed by Novogene Bioinformatics Technology Co., Ltd. (Beijing, China).

Low expression genes were filtered out using a threshold of >1 FPKM in all three replicates in either 293T WT or ΔUBR5 samples. Two independent biological replicates (each with three replicates) were combined by taking, for each gene, the mean of the average expression fold change from each biological replicate and the geometric mean of their individual p-values computed from DESEQ2. Transcript length is defined as the abs(start gene coordinate - end gene coordinate). To analyze statistical enrichment of genes differentially expressed based on transcript length, we computed the Fisher's exact test at each transcript length (above or below) comparing the number of differentially expressed genes (as defined by a $\log_2$(fold change)>1 or <-1 and p-value<0.05) above (or below) a given transcript length, to the total number of genes. We defined Myc genes from ChIP-seq enrichment using ENCODE ChIP-seq datasets ENCFF270GMO, ENCFF784BWK and ENCFF608CXN, whose peaks were mapped to genes using ChIP-seeker. Statistical enrichment/depletion of Myc genes in differentially expressed genes was computed from Fisher's exact test.

Cryo electron microscopy

UBR5 and MCRS1 full-length proteins were mixed at ~15 μM and ~45 μM, respectively. Following a short incubation time of 5 minutes on ice, the sample was applied to a 10-40% glycerol gradient based on 20 mM HEPES pH 7.6, 150 mM NaCl, 0.5 mM TCEP and 0.15% glutaraldehyde (Science Services, E16220) according to the "GRAFIX" method.[97] The gradient was ultracentrifuged at 33 K rpm and 4°C for 14 hours in a SW-60 Ti swinging-bucket rotor (Beckmann Coulter, 335650). Subsequently, the gradient was harvested top-down by piston fractionation and monitoring the peak fractions by the 280 nm absorbance trace. Peak fractions were pooled with subsequent buffer exchange using Zeba-spin desalting columns (40K MWCO, Thermo Fisher, 87767) into buffer without glycerol (20 mM HEPES pH 7.6, 150 mM NaCl, 0.5 mM TCEP). Finally, the sample was concentrated to ~20 μL using an Amicon centrifugal filter concentrator (30 kDa MWCO, Merck-Millipore, UFC5030).

For grid preparation, 4 μL of sample were applied to glow-discharged UltrAuFoil 1.2/1.3 300-mesh gold grids (Quantifoil Micro Tools, N1-A14nAu30-01). A Vitrobot Mark IV (FEI) was used for plunge freezing into liquid ethane after a 3 seconds blot time at 95% humidity and 4°C.

Data were collected on a Cs-corrected (CEOS GmbH, Heidelberg, Germany) Titan Krios electron microscope (Thermo Fisher) operating at 300 kV. Automatic data collection were performed using the EPU software (Thermo Fisher) at a nominal magnification of 75,000x, corresponding to a pixel size of 0.845 Å. Movies were recorded with a Falcon 4 direct electron detector (Thermo Fisher) in 50 frames with a total electron dose of 50 $e^-/Å^2$ and 1 $e^-/Å^2$ per frame. For data collected at a stage tilt of 30°, a total electron dose of 55 $e^-/Å^2$ and 1.1 $e^-/Å^2$ per frame was used instead. Defocus values ranged from −1.0 to −2.2 μm. Real-time evaluation was performed with CryoFLARE.[98] Motion correction of the collected images was performed with motioncorr implemented in Relion 3. All

subsequent processing steps were performed in cryoSPARCv4,[99] with additional details illustrated in Figure S7. Reported resolution values are based on the gold-standard Fourier shell correlation (FSC) curve at 0.143 criterion.[100] High-resolution noise substitution was used for correcting the effects of soft masking for the related FSC curve. Local resolution was estimated in cryoSPARCv4. The map was subjected to amplitude-scaling using LocScale.[101]

Integrative model building

The predicted structure of MCRS1 was obtained from the AlphaFold Database (AF-Q96EZ8-F1-model_v4).[102] For docking, the MCRS1 model was truncated to aa 335-461. The UBR5 model was obtained from a parallel study. The MCRS1 and UBR5 models were fit into the cryoEM map using ChimeraX fit-in-map[103] and combined. The Rosetta 3 Docking Protocol[104] was used to dock MCRS1 against the UBR5 HECT domain since the limited local resolution did not permit unambiguous fitting of MCRS1. The extracted complex was prepacked and subjected to the ''low resolution'' docking protocol in centroid representation, including random perturbations of the MCRS1 chain (*randomize2* and *spin* keywords) around UBR5-HECT. After this step, filtering was performed based on the crosslink set, allowing a maximum distance of 30 Å. Only crosslinked UBR5 lysines that would be solvent accessible from the observed MCRS1 cryo-EM density (irrespective of MCRS1 orientation) were considered (selected crosslinks with UBR5<->MCRS1 residue numbers: 2792<->458, 2786<->458, 2780<->458, 2786<->390, 2786<->397). This was followed by ''high resolution'' docking in full atom representation in combination with local perturbations of 3 degrees and 8 Å. The resulting poses were subjected to another round of filtering as described above. Finally, poses were scored against the cryo-EM map using the elec_dens_fast function. The full protocol was run with 2000 attempts yielding 102 poses that passed all filtering criteria. The interface score (I_sc) was plotted against the density score (elec_dens_fast) and the final pose was selected from the top 2 poses based on best I_sc and elec_dens_fast scores (50% weight of each score).

The selected docking pose was merged into the full UBR5 model using the HECT domain as superposition reference. The combined model was subjected to flexible fitting with Isolde[105] applying tight self-restraints. Finally, the model coordinates and B-factors were refined with Phenix real_space_refinement[106] applying tight coordinate restraints. Side chains were removed and MCRS1 was truncated to aa 346-460. The figures were made with PyMOL (Schrödinger, LLC) and ChimeraX.

Crosslinking Mass spectrometry (XL-MS)

The recombinantly expressed UBR5 HECT domain (2216-2799) and STREP-SUMO-MCRS1 (294-462) were mixed in an equimolar ratio (820 pmol) to a total protein amount of 60 μg in 50 mM HEPES pH 7.5, 150 mM NaCl, 0.5 mM TCEP and incubated with 1.6 mM DSSO (Disuccinimidyl sulfoxide, Thermo Fisher Scientific, A33545) for 1 hour at 10°C and 400 rpm. The reaction was quenched with 50 mM Tris-HCl pH 6.8 for an additional 1 hour while shaking at 400 rpm at room temperature. The cross-linked sample was transferred to an Amicon centrifugal filter concentrator (3 kDa MWCO, Merck-Millipore, UFC5003) to remove excess DSSO, followed by washing in 400 μl of XL buffer (8 M urea in 50 mM HEPES pH 8.5) to denature the proteins. The washing was repeated twice and finally concentrated to 50 μl. Alkylation was performed using 10 mM 2-chloroacetamide (CAA) and 5 mM TCEP in 8 M Urea for 30 minutes at 400 rpm in the dark. The sample was washed three times in XL buffer and finally concentrated to 50 μl. The sample was diluted to 6 M urea and digested by Lys-C addition (1:75 enzyme to protein ratio, FUJIFILM Wako Chemicals, 125-05061) for 4 hours at 37°C and 400 rpm. The sample was further diluted to 2 M urea, followed by adding Trypsin (1:50 ratio, Promega, V5111) and digestion overnight at 37°C and 400 rpm. Again, Trypsin in a 1:50 ratio was added with acetonitrile to a final concentration of 5% with subsequent incubation for another 4 hours at 37°C. The sample was transferred into an Eppendorf tube. 5 uL 50% TFA were added for a final pH of ca. 3, and the sample was sonicated and spun down for 5 minutes at 20,000 g. The supernatant was desalted using a PreOmics iST-NHS kit (PREOMICS, P.0.00030) and concentrated in a speedvac. Samples were reconstituted with 0.1% TFA in 2% acetonitrile. The equivalent of ca. 5 ug peptides were loaded onto a Vanquish Neo chromatography system with two-column setup onto a trapping column at a constant pressure of 800 bar. Peptides were chromatographically separated at a flow rate of 250 nl/min using a 142 min method, with a linear gradient of 2-7% B in 4 min, followed by 7-20% B in 78 min, 20-30% B in 30 min, 30-36% B in 12 min, 36-45% B in 4 min, and finally 45-100% B in 4 min, and finally washing for 10 min at 100% B (Buffer A: 0.1% formic acid; buffer B: 0.1 formic acid in 80% acetonitrile) on a 15 cm EASY Spray Neo C18 HPLC column mounted on an EASY-Spray source connected to an Orbitrap Eclipse mass spectrometer with FAIMS (all Thermo Fisher Scientific). Three experiments were defined in the MS method, with three different FAIMS compensation voltages, -50, -60 and -75 V, respectively, to increase the chances for more highly charged peptides, i.e., crosslinked peptides, to be identified. For each experiment, peptide MS1 precursor ions were measured in the Orbitrap at 60k resolution. The MS' Advanced peak determination (APD) feature was enabled, and those peptides with assigned charge states between 3 and 8 were subjected to CID–MS2 fragmentation (25% CID collision energy), and fragments detected in the Orbitrap at 30 k resolution. Data-dependent HCD-MS3 scans were performed if a unique mass difference (Δm) of 31.9721 Da was found in the CID–MS2 scans with detection in the ion trap (35% HCD collision energy).

MS raw data were analyzed in Proteome Discoverer version 2.5 (Thermo Fisher Scientific) using a Sequest database search for linear peptides, including crosslinker-modifications, and an XlinkX search to identify cross-linked peptides. MS2 fragment ion spectra not indicative of the DSSO crosslink delta mass were searched with the Sequest search engine against a custom protein database containing the expected protein components, as well as a database of contaminants commonly identified during in-house analyses, from MaxQuant, and cRAP (ftp://ftp.thegpm.org/fasta/cRAP), using the target-decoy search strategy. The following variable crosslinker modifications were considered: DSSO Hydrolyzed/+176.014 Da (K); DSSO Tris/+279.078 Da (K), DSSO

alkene fragment/+54.011 Da (K); DSSO sulfenic acid fragment/+103.993 Da (K), as well as Oxidation/+15.995 Da (M). Carbamidomethyl/+57.021 Da (C) was set as a static modification. Trypsin was selected as the cleavage reagent, allowing a maximum of two missed cleavage sites, peptide lengths between 4 or 6 and 150, 10 ppm precursor mass tolerance, and 0.02 Da fragment mass tolerance. PSM validation was performed using the Percolator node in PD and a target FDR of 1%. XlinkX was used to perform a database search against a custom protein database containing the expected complex components to identify DSSO-crosslinked peptides and the following variable modification: DSSO Hydrolyzed/+176.014 Da (K); Oxidation/+15.995 Da (M). Crosslink-to-spectrum matches (CSMs) were accepted above an XlinkX score of 40. Crosslinks were grouped by sequences and link positions and exported to xiNET format together with a fasta database containing all crosslinked proteins to generate cross-link network maps. The cross-links with a score above 50 were displayed using the xiNET visualization tool.[107]

QUANTIFICATION AND STATISTICAL ANALYSIS

All quantifications are presented as the mean ± standard deviation. Significance was determined by two-tailed t test, ns $p > 0.05$ and significant $p \leq 0.05$. The top 21 hits from the flow cytometry screen in Figure 2A were performed in biological triplicate and plotted as the mean median fold change. RNA-seq experiments in Figures 4A and S4A were performed in biological triplicate. All RT-qPCR quantifications are presented as the mean of three independent biological replicates ± standard deviation.

CellPress
OPEN ACCESS

Supplemental figures

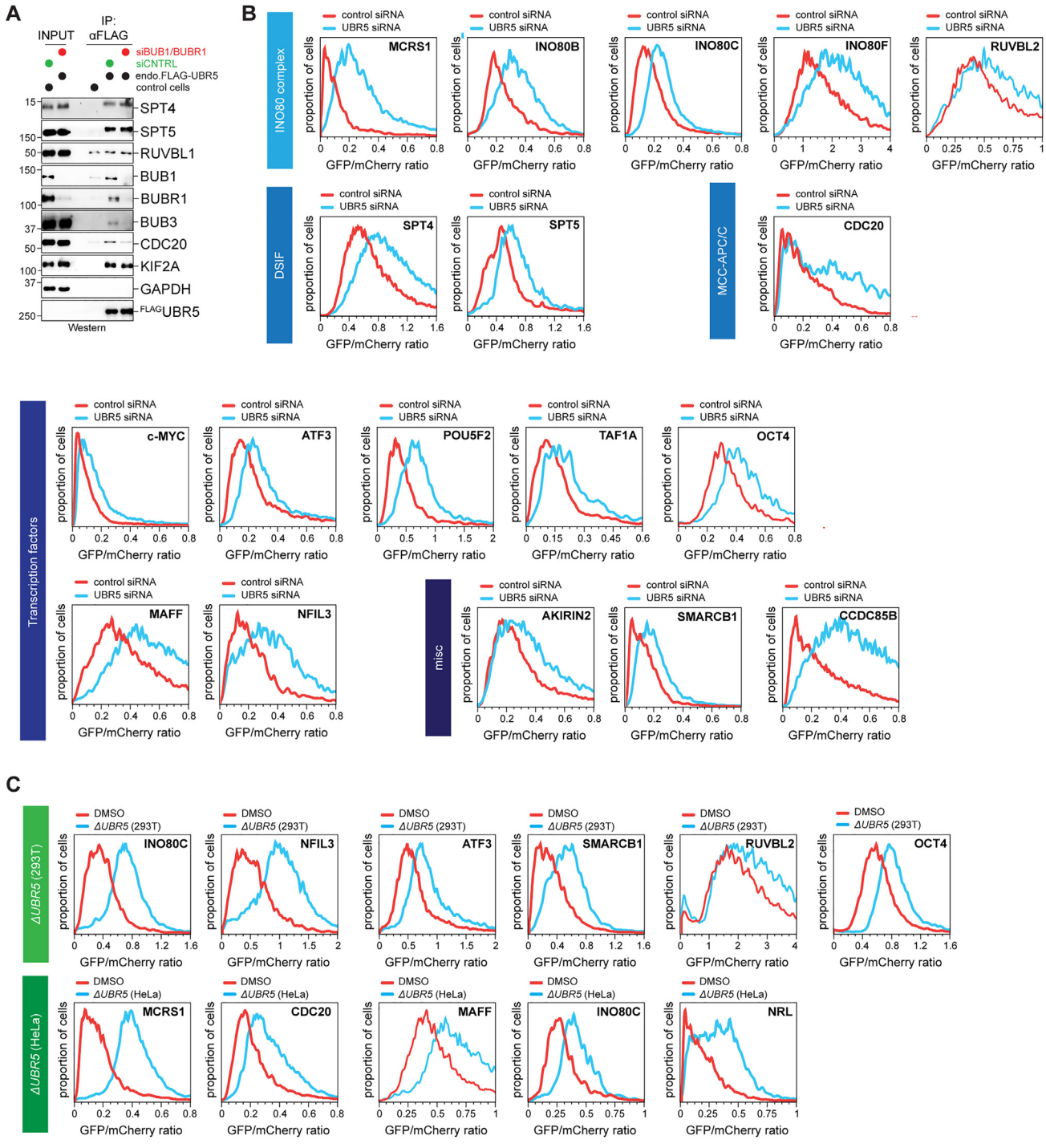

Figure S1. Validation of UBR5 substrate screen, related to Figures 1 and 2

(A) Depletion of BUB1 and BUBR1 reduces MCC subunits in the affinity purifications of endogenous ^{FLAG}UBR5 from HeLa cells.

(B) Validation of substrate screen in HeLa cells treated with siRNAs targeting UBR5. Reporter stability was measured by flow cytometry.

(C) Validation of UBR5 screen for select substrates in *ΔUBR5* (293T) and *ΔUBR5* (HeLa) cells.

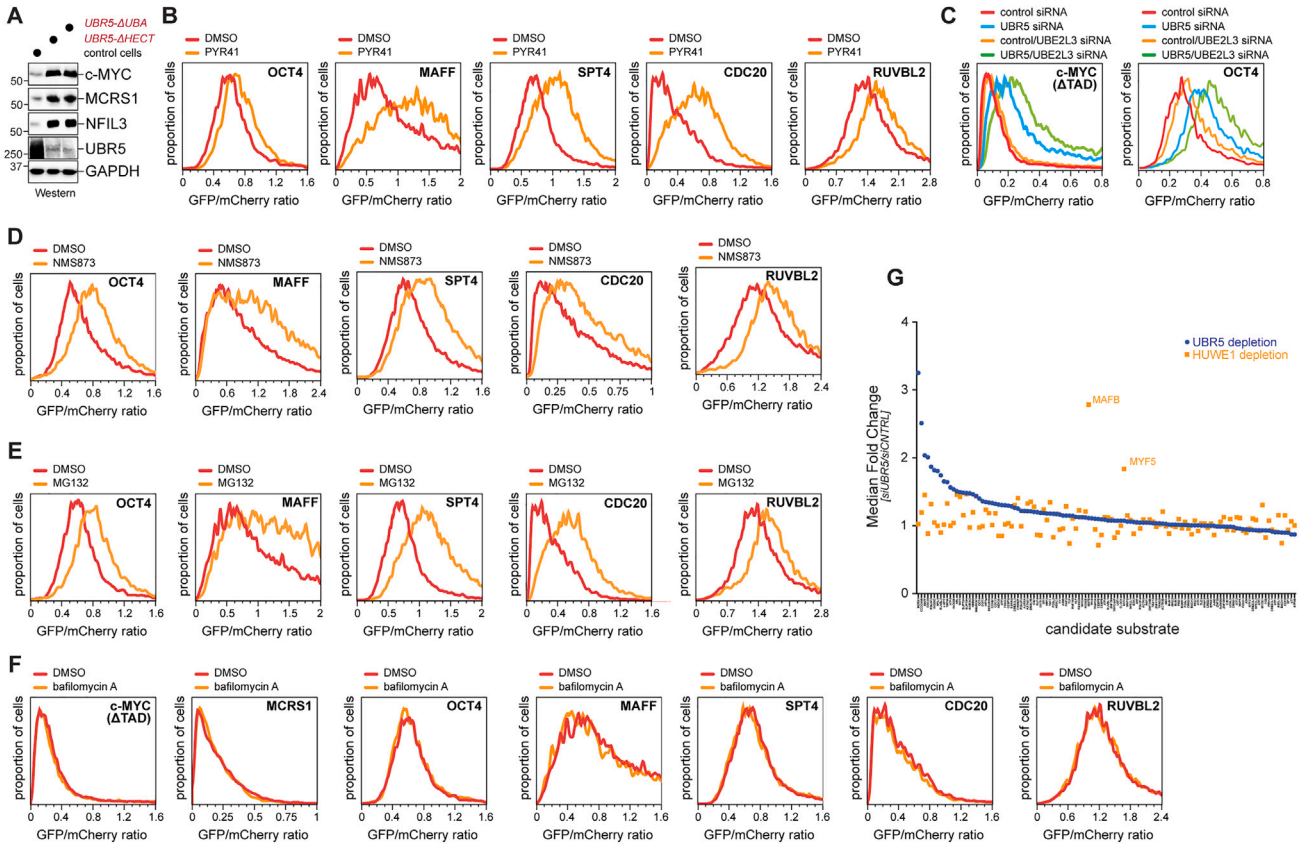

Figure S2. Specificity of UBR5 substrate degradation, related to Figure 2

(A) Endogenous UBR5 targets increase in HeLa cells with the deletions of the UBR5 HECT and UBA domains, as determined by western blot analysis.

(B) Select substrates are stabilized upon E1 enzyme inhibition by PYR41.

(C) Cells were treated with control siRNAs, UBR5 or UBE2L3 siRNAs, or both. Reporter stability was measured by flow cytometry.

(D) Substrates are stabilized by p97 inhibition with NMS873.

(E) Substrates are stabilized by proteasome inhibition with MG132.

(F) Lysosome inhibition does not affect substrate stability.

(G) Flow cytometry-based stability screen in cells treated with siRNAs targeting HUWE1.

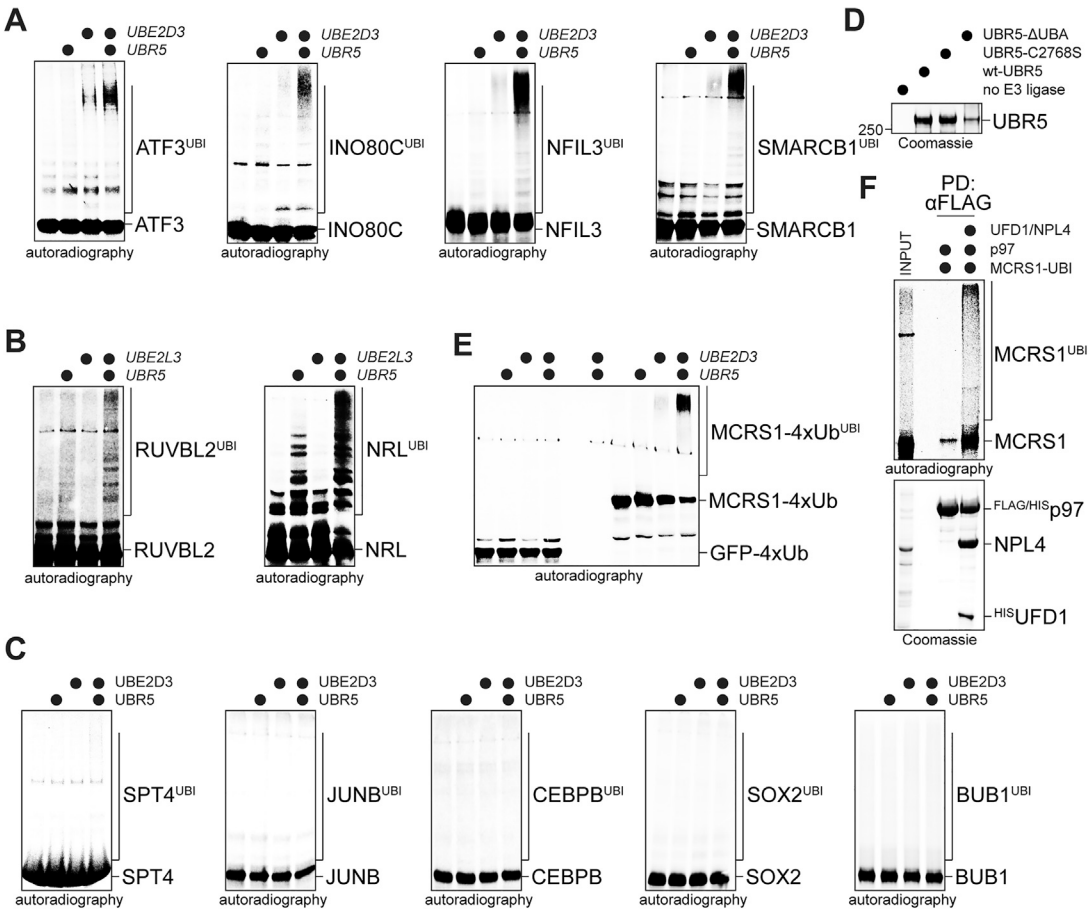

Figure S3. UBR5 ubiquitylates transcriptional regulators, related to Figure 3

(A) *In vitro* ubiquitylation of candidate ^{35}S-labeled substrates by UBR5 and UBE2D3.

(B) ^{35}S-labeled targets were incubated with UBR5, E1, UBE2L3, and ubiquitin and analyzed as above.

(C) ^{35}S-labeled SPT4 and several control proteins were incubated with UBR5, E1, UBE2D3, and ubiquitin and analyzed as above.

(D) Purification of UBR5 and indicated mutants from HeLa cells.

(E) GFP∼Ub4 (four ubiquitin moieties fused to GFP) or MCRS1∼Ub4 were incubated with UBR5, E1, UBE2D3, and ubiquitin and analyzed for ubiquitylation.

(F) Purified recombinant p97, UFD1, and NPL4 were incubated with the MCRS1 that had been ubiquitylated by UBR5 *in vitro* and analyzed by autoradiography.

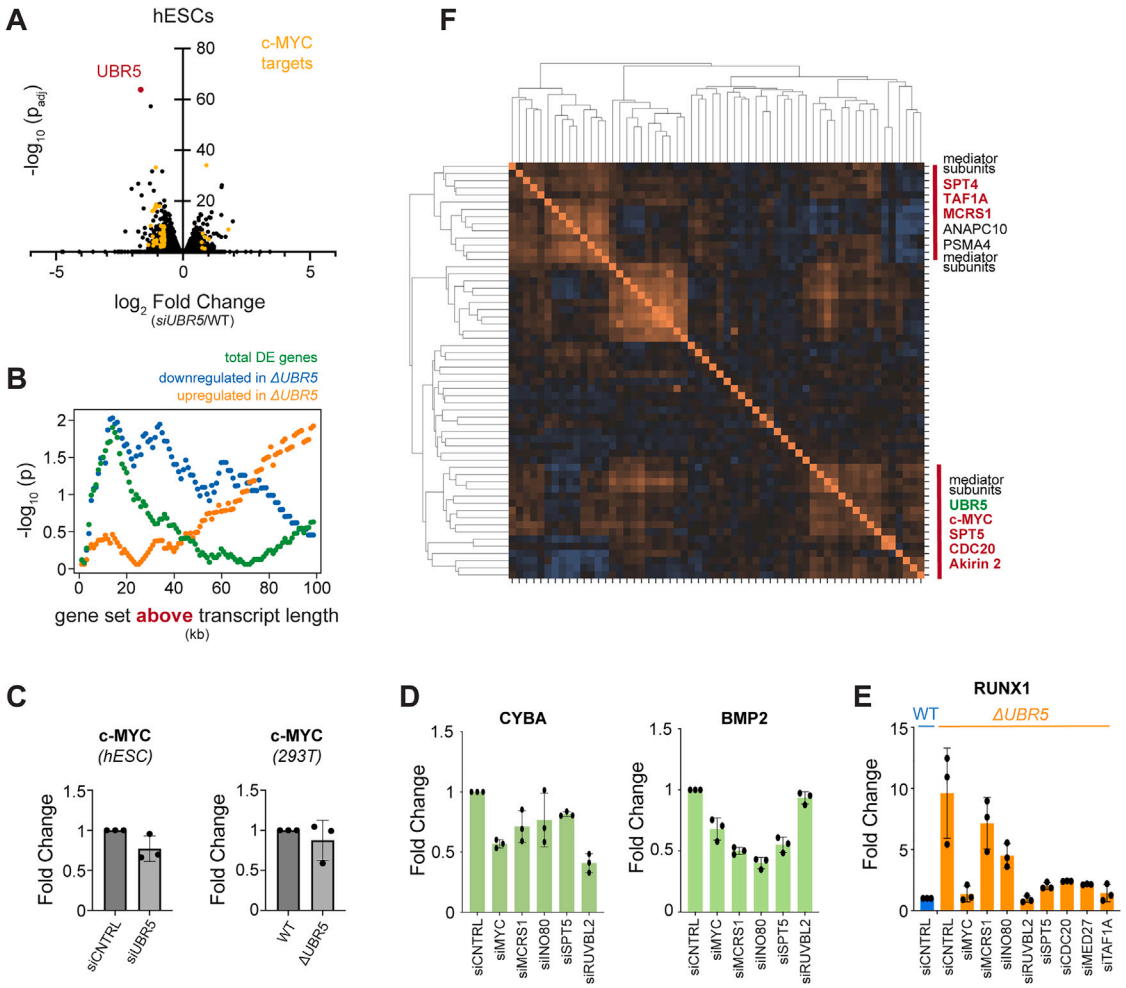

Figure S4. UBR5 targets are required for accurate gene expression, related to Figure 4

(A) RNA-seq analysis after brief UBR5 depletion in hESCs.

(B) Likelihood that genes above a certain transcript length threshold are upregulated in *ΔUBR5* 293T cells.

(C) Expression of c-Myc is not altered in hESCs or 293T cells lacking UBR5, as determined by qRT-PCR. Data are represented as mean ± SD.

(D) Depletion of UBR5 substrates reduces the expression of *CYBA* and *BMP2*, as determined by qRT-PCR. Data are represented as mean ± SD.

(E) Depletion of UBR5 substrates blunts the effect of *UBR5* deletion on the expression of RUNX1. Data are represented as mean ± SD.

(F) Heatmap showing DepMap correlations among UBR5, select substrates, and the mediator complex.

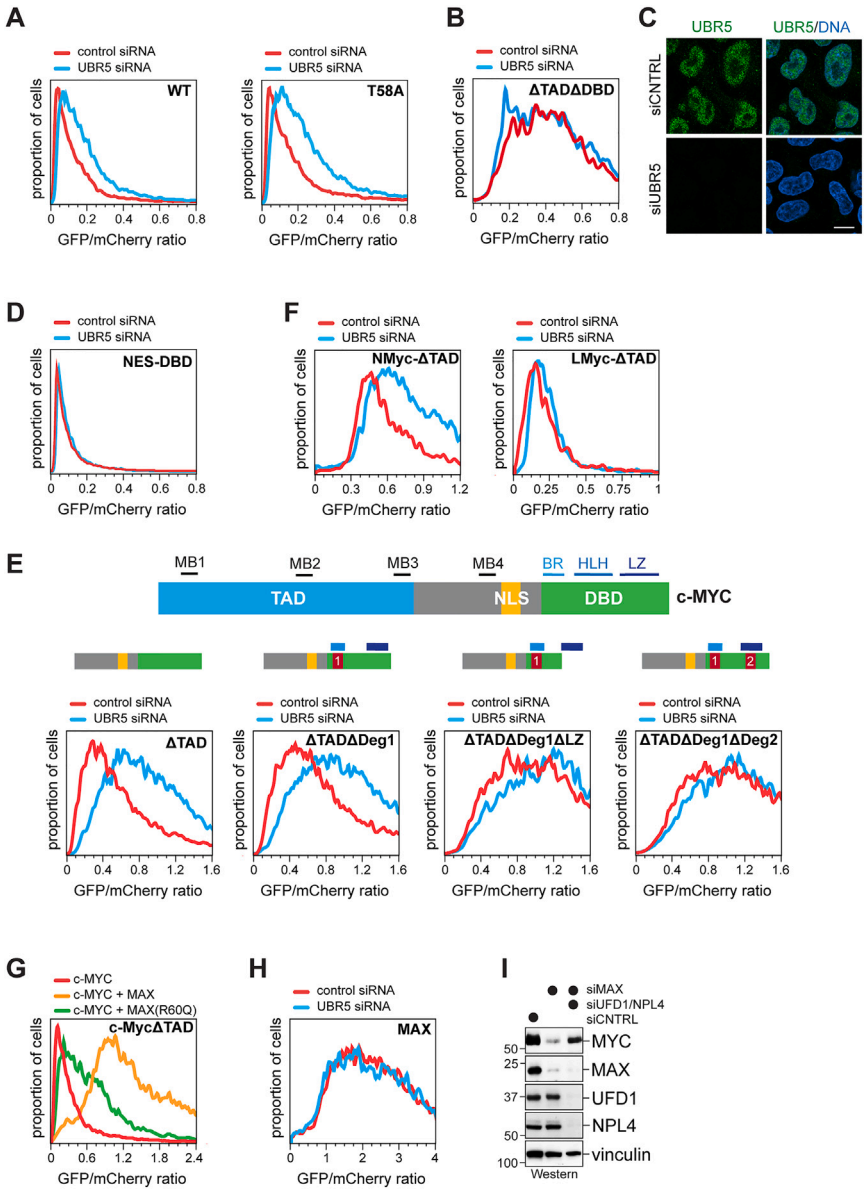

Figure S5. UBR5 targets orphan c-Myc, related to Figure 5

(A) Stability of c-Myc or c-Myc^{T58A} in cells depleted of UBR5 siRNA was measured by flow cytometry.

(B) A c-Myc$^{\Delta TAD\Delta DBD}$ reporter was analyzed in UBR5-depleted cells.

(C) Localization of endogenous ^{FLAG}UBR5 was determined in HeLa cells by microscopy (scale bars, 10 μM).

(D) Stability of c-Myc^{DBD} fused to a nuclear export signal (NES) was measured in UBR5-depleted cells by flow cytometry.

(E) GFP-tagged reporters containing the carboxy-terminal half of c-Myc (ΔTAD) and mutations in degron 1 (ΔTADΔDeg1), leucine zipper (ΔTADΔDeg1ΔLZ), or both degrons (ΔTADΔDeg1ΔDeg2) were expressed in cells treated with siRNAs targeting UBR5.

(F) Reporters containing NMYC-ΔTAD or LMYC-ΔTAD were expressed in cells treated with control siRNA or siRNAs targeting UBR5.

(G) MAX^{R60Q}, which forms fewer dimers with c-Myc, is also less efficient in stabilizing a c-Myc$^{\Delta TAD}$ reporter than WT-MAX.

(H) MAX is not degraded by UBR5.

(I) Co-depletion of p97 adaptors rescues c-Myc levels in cells depleted of MAX, as determined by western blot analysis.

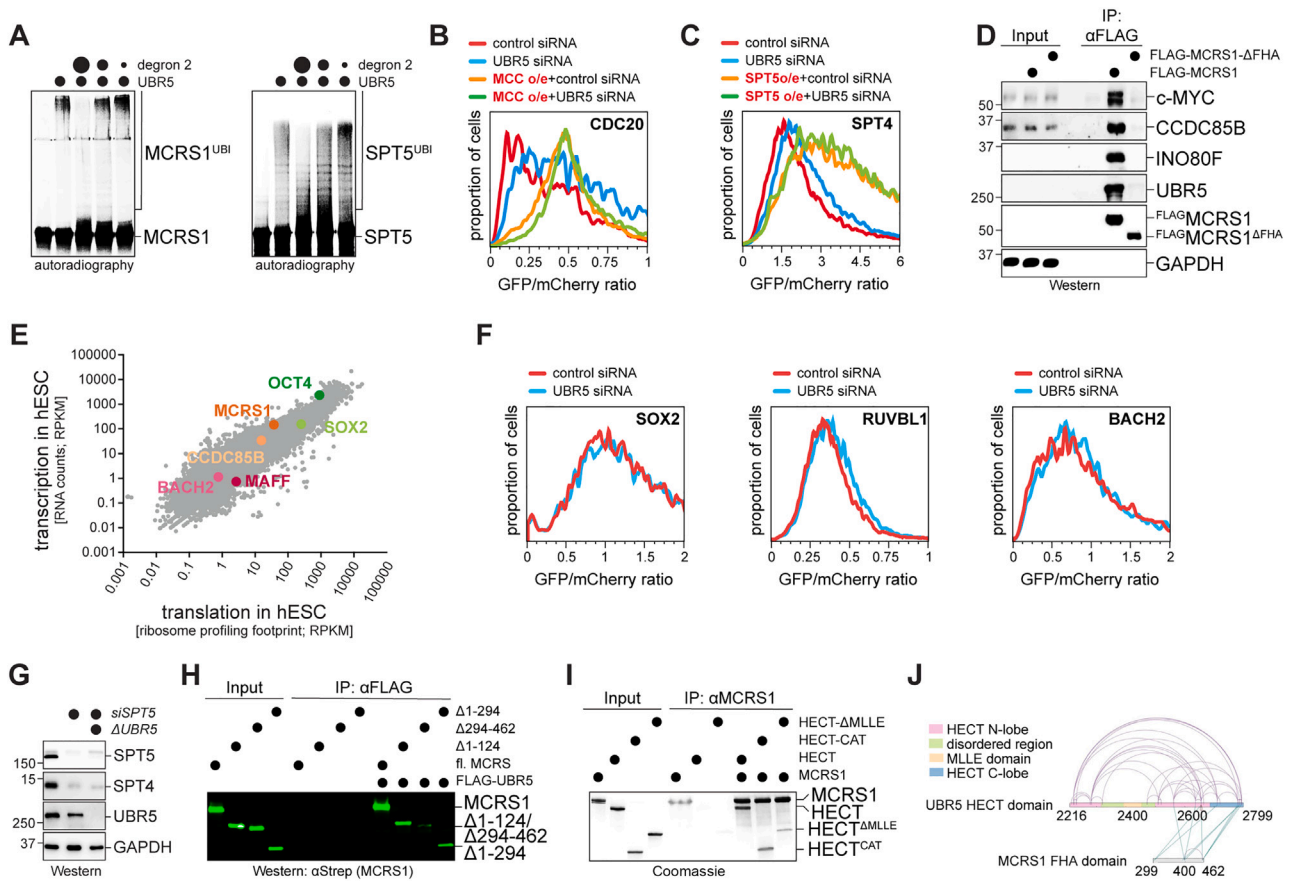

Figure S6. Complex formation stabilizes UBR5 targets, related to Figure 6

(A) Ubiquitylation of ^{35}S-labeled MCRS1 or SPT5 was monitored in the presence of increasing concentrations of c-Myc degron-2 by autoradiography.

(B) MCC components protect a CDC20^{GFP}::mCherry reporter from degradation.

(C) SPT4 is more extensively stabilized upon the co-expression of SPT5 than upon UBR5 depletion.

(D) ^{FLAG}MCRS1 and ^{FLAG}MCRS1$^{\Delta FHA}$ were purified from 293T cells and analyzed for interactors by western blot analysis.

(E) UBR5 substrates are expressed in large excess over stabilizing partners in hESCs, as shown by RNA-seq and ribosome profiling.

(F) SOX2, RUVBL1, and BACH2, are not significantly stabilized by UBR5 depletion.

(G) Wild-type or *ΔUBR5* 293T cells were depleted of SPT5, and SPT4 levels were determined by western blot analysis.

(H) The carboxy-terminal domain of MCRS1 is required for its recognition by purified UBR5, as detected by Western.

(I) The HECT domain of UBR5 is sufficient to mediate binding to MCRS1 *in vitro*.

(J) Crosslink mass spectrometry experiments help determine the orientation of MCRS1 on UBR5.

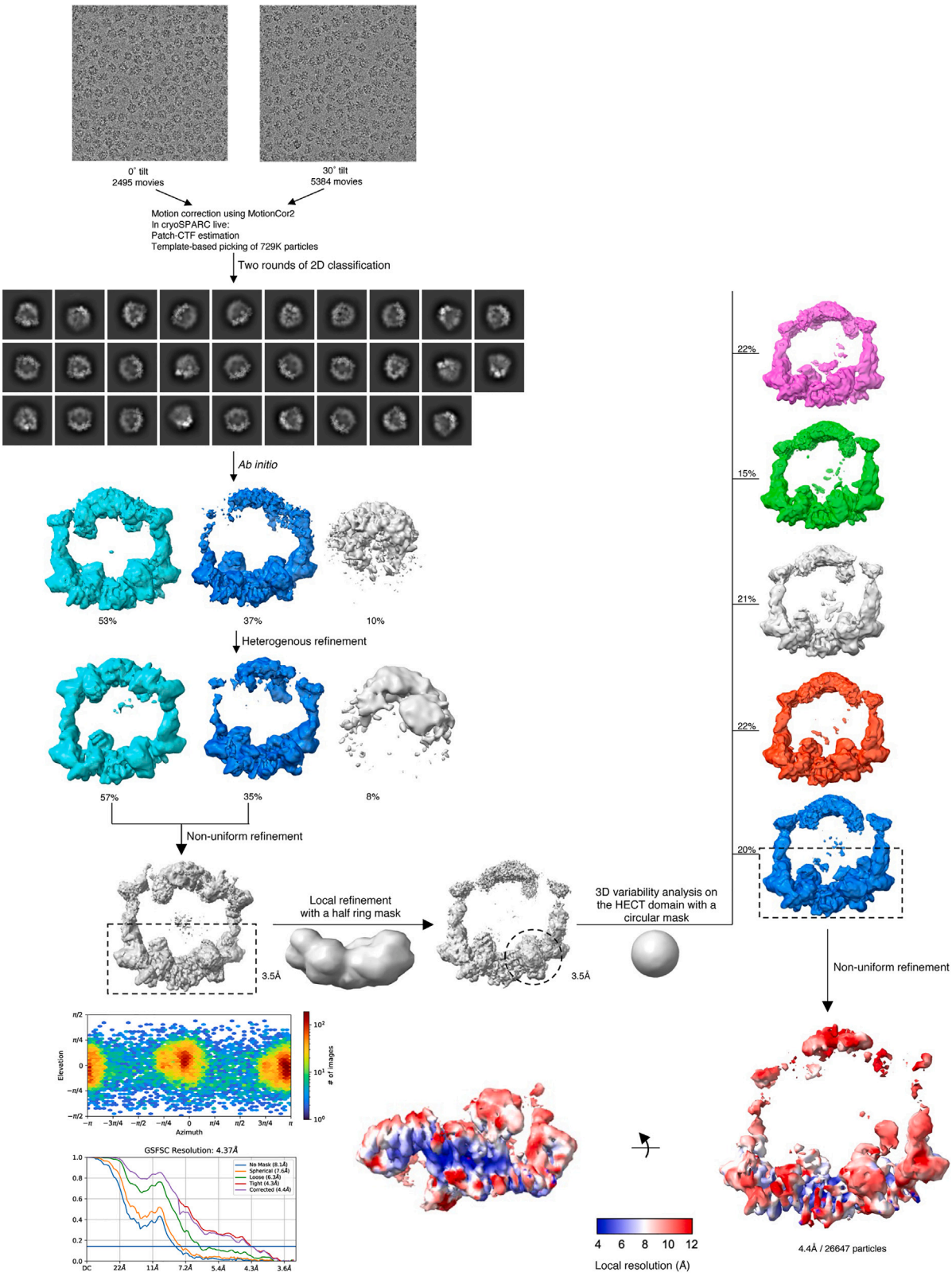

(legend on next page)

Figure S7. Data processing pipeline for UBR5~MCRS1 structure, related to Figure 6

Data processing pipeline for UBR5∼MCRS1 structure. All data were processed entirely in cryoSPARC v3. Representative motion-corrected micrographs are shown at the top. Stage-tilted (30°) and non-tilted (0°) datasets were imported into cryoSPARC and motion corrected, and CTF estimation was performed in patch mode. Subsequent *ab initio*, classification, and refinement steps are shown. The final models are presented in 2 orientations and colored by local resolution. Viewing angle distribution maps and gold-standard Fourier shell correlation (GSFSC) curves are shown after Fourier shell correlation (FSC) mask auto-tightening for the final models.

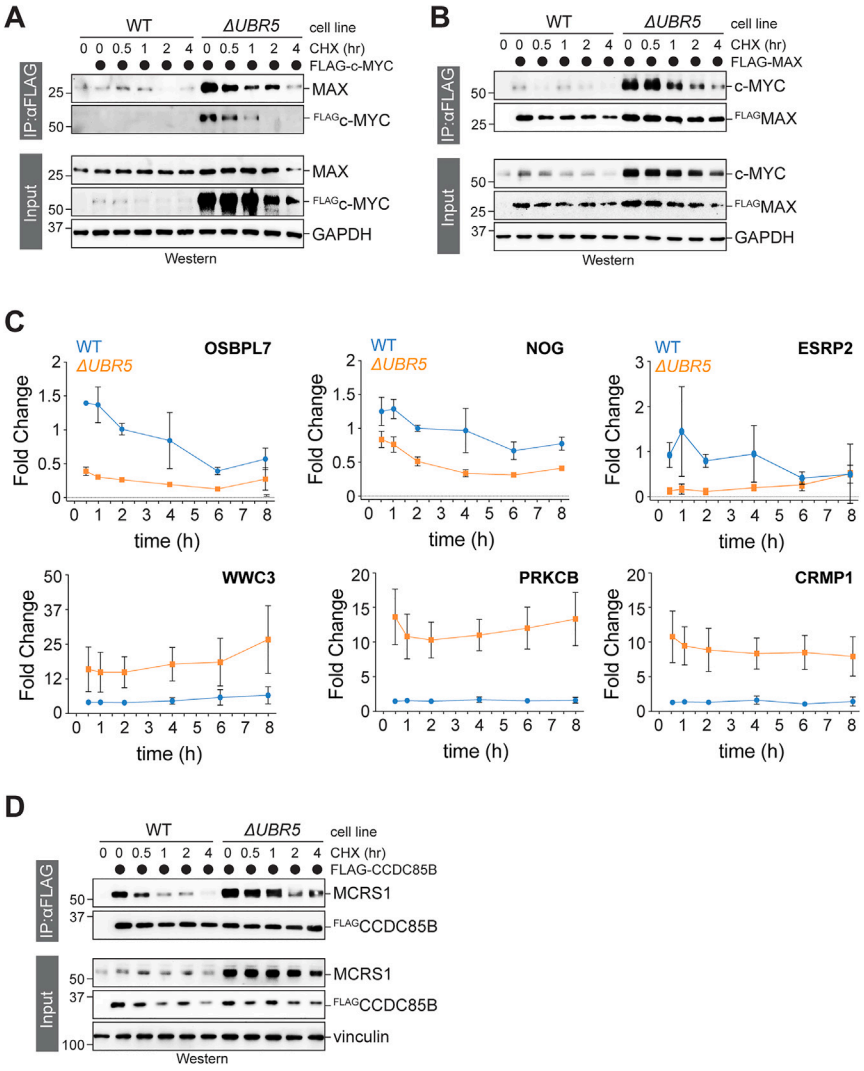

Figure S8. Orphan protein degradation regulates complex stability, related to Figure 7

(A) *ΔUBR5* cells were transfected with ^{FLAG}c-Myc and treated with cycloheximide as indicated. ^{FLAG}c-Myc was immunoprecipitated, and co-purifying MAX was detected by western blot analysis.

(B) Wild-type or *ΔUBR5* HeLa cells expressing ^{FLAG}MAX were treated with cycloheximide. ^{FLAG}MAX was immunoprecipitated, and co-purifying proteins were detected by western blot analysis.

(C) Gene expression was analyzed in wild-type or *ΔUBR5* cells after oligomycin and antimycin A treatment using qRT-PCR. Data are represented as mean ± SD.

(D) Control or *ΔUBR5* HeLa cells were transfected with ^{FLAG}CCDC85B and treated with cycloheximide. ^{FLAG}CCDC85B was immunoprecipitated, and co-purifying MCRS1 was detected by western blot analysis.